Redox Biology 40 (2021) 101839

Contents lists available at ScienceDirect

Redox Biology

journal homepage: www.elsevier.com/locate/redox

Research Paper

Cell-penetrating, antioxidant SELENOT mimetic protects dopaminergic neurons and ameliorates motor dysfunction in Parkinson's disease animal models

Ifat Alsharif[a,b,c,1], Loubna Boukhzar[a,b,1], Benjamin Lefranc[a,b,d], David Godefroy[a,b], Juliette Aury-Landas[e], Jean-Luc do Rego[b,f], Jean-Claude do Rego[b,f], Frédéric Naudet[g], Arnaud Arabo[h], Abdeslam Chagraoui[a,b], David Maltête[a,b], Abdelhamid Benazzouz[g], Catherine Baugé[e], Jérôme Leprince[a,b,d], Abdel G. Elkahloun[i], Lee E. Eiden[j], Youssef Anouar[a,b,*]

[a] UNIROUEN, Inserm U1239, Neuronal and Neuroendocrine Differentiation and Communication Laboratory, Rouen Normandie University, 76821, Mont-Saint-Aignan, France
[b] Institute for Research and Innovation in Biomedicine, 76000, Rouen, France
[c] Biology department, Jamoum University College, Umm Alqura University, Saudi Arabia
[d] PRIMACEN, Cell Imaging Platform of Normandie, UNIROUEN, 76000, Rouen, France
[e] UNICAEN, BioConnecT EA7451, 14000, Caen, France
[f] Behavioral Analysis Platform SCAC, Rouen Medical School, Rouen Normandie University, 76183, Rouen, France
[g] Institut des Maladies Neurodégénératives, CNRS, UMR 5293, Bordeaux University, F-33000, Bordeaux, France
[h] Biological Resource Service (SRB), Faculty of Sciences and Techniques, Rouen Normandie University, 76821, Mont-Saint-Aignan, France
[i] Comparative Genomics and Cancer, Genetics Branch, National Human Genome Research Institute, National Institutes of Health, Bethesda, MD, USA
[j] Section on Molecular Neuroscience, National Institute of Mental Health Intramural Research Program, National Institutes of Health, Bethesda, MD, USA

ARTICLE INFO

Keywords:
Selenoprotein
Peptide therapy
Neurodegenerative disease
Oxidative stress
Neuron

ABSTRACT

Parkinson's disease (PD) is a neurodegenerative disorder characterized by motor dysfunction for which there is an unmet need for better treatment options. Although oxidative stress is a common feature of neurodegenerative diseases, notably PD, there is currently no efficient therapeutic strategy able to tackle this multi-target pathophysiological process. Based on our previous observations of the potent antioxidant and neuroprotective activity of SELENOT, a vital thioredoxin-like selenoprotein, we designed the small peptide PSELT from its redox active site to evaluate its antioxidant properties *in vivo,* and its potential polyfunctional activity in PD models. PSELT protects neurotoxin-treated dopaminergic neurons against oxidative stress and cell death, and their fibers against neurotoxic degeneration. PSELT is cell-permeable and acts in multiple subcellular compartments of dopaminergic neurons that are vulnerable to oxidative stress. In rodent models of PD, this protective activity prevented neurodegeneration, restored phosphorylated tyrosine hydroxylase levels, and led to improved motor skills. Transcriptomic analysis revealed that gene regulation by PSELT after MPP^+ treatment negatively correlates with that occurring in PD, and positively correlates with that occurring after resveratrol treatment. Mechanistically, a major impact of PSELT is via nuclear stimulation of the transcription factor EZH2, leading to neuroprotection. Overall, these findings demonstrate the potential of PSELT as a therapeutic candidate for treatment of PD, targeting oxidative stress at multiple intracellular levels.

* Corresponding author. Lab. Neuronal and Neuroendocrine Differentiation and Communication, INSERM U1239, University of Rouen Normandie, 25 rue Tesnière, 76821, Mont-Saint-Aignan, France.
E-mail address: youssef.anouar@univ-rouen.fr (Y. Anouar).
[1] Contributed equally and should be considered joint first authors.

https://doi.org/10.1016/j.redox.2020.101839
Received 22 October 2020; Received in revised form 10 December 2020; Accepted 15 December 2020
Available online 28 December 2020

1. Introduction

Parkinson's disease (PD) is an idiopathic chronic movement disorder of adults that afflicts 1–2% of persons over 65 years of age [1]. Cardinal signs of this disease include bradykinesia, rest tremor, and limb and axial rigidity, which collectively reduce life expectancy [2]. Motor symptoms are the consequence of progressive loss of dopaminergic neurons of the substantia nigra pars compacta (SNc) projecting to the striatum [3]. In the 200 years since the description of the disease, its etiology is increasingly appreciated to be a cascade comprising multiple factors converging on cumulative insult to dopaminergic neurons. Impairment of several major cellular processes including proteostasis, mitochondrial activity and redox regulation are likely to converge to produce dopamine neuronal damage and the progressive symptoms of PD [4–6]. Extensive postmortem studies have provided evidence to support the involvement of oxidative stress in the pathogenesis of PD [7–9]. It is now well established that aging dopaminergic neurons of the SN have high basal levels of reactive oxygen species (ROS) which confer vulnerability to oxidative insult provoked by further oxidative stress in PD. This pathogenic ROS-induced stress leads to DNA damage, lipid peroxidation, protein modification and other pathological effects ultimately causing cellular damage and demise.

Despite this mechanistic understanding of PD progression and disease, attempts to translate therapeutics based on antioxidants such as vitamins C and E, and glutathione, or redox elements like selenium and zinc, have been relatively unsuccessful [10,11].These may be explicable in part by a need for some specificity in antioxidant action in PD, since antioxidants which act solely as ROS scavengers may not revert the cell-specific harmful effects of ROS on cellular constituents in dopaminergic neurons, and may even have deleterious effects by suppressing ROS levels necessary for various normal physiological functions [12]. Other potential therapeutics which target a cellular compartment, *e.g.* mitochondria or endoplasmic reticulum (ER) [13,14] or one of the enzymes involved in redox homeostasis [15] may in fact be limited by their specificity, since oxidative stress is a multi-target pathological process. Accordingly, agents acting against oxidative stress tailored more closely to the recovery of the integrity of cell components in neurons, if identified, could be broadly useful in treatment of neurodegeneration in PD and other neurodegenerative diseases.

Neuropathological observations in early-stage PD patients point to elevated oxidative stress as a robust feature of initial disease stages preceding significant neuron loss [7,16,17]. In the aging SNc, several factors converge to exacerbate oxidative stress and weaken the physiological antioxidant defense system. The latter relies on an arsenal of enzymes and factors including selenoproteins, the antioxidant selenium-containing proteins with key defense functions in plasma membrane, nucleus, and other subcellular organelles [18]. Selenoproteins are involved in key cellular processes, including redox equilibrium, Ca^{2+} homeostasis, protein folding and cell survival, which are known to be deregulated in neurodegenerative diseases and particularly in PD [19,20]. These several compartments and pathways, that could be affected by oxidative stress, all provide points of entry for development of new multi-system redox active therapeutics. We and others have shown that selenoproteins play a key function in the protection of dopaminergic neurons [21–25], and may thus serve as a basis for therapeutic protection of these neurons. In particular, we have recently shown that selenoprotein T (SELENOT), whose gene disruption is lethal in mice [21,26], promotes dopaminergic neuron survival and contributes to normal motor function [21,27,28]. SELENOT is able to reduce free radical level and to prevent ER stress [21,27,29], most probably by reducing disulfide bridges during glycoprotein synthesis and folding although its precise mechanism of action in dopaminergic neurons is not known yet.

SELENOT belongs to a group of ER-resident redoxins which harbor a thioredoxin motif carrying the catalytic activity and including a CXXU amino acid sequence where U is a selenocysteine (Sec) that can form a selenosulfide bridge with the upstream Cys residue. This motif is able to interact with other cellular components via redox reactions [26,30]. Based on this knowledge, we reasoned that a short peptide encompassing this motif could exert a protective effect that would mimic several redoxins acting at different levels in neurons. The peptide PSELT, with the sequence FQICVSUGYR, was designed and synthesized to test this hypothesis. Here, we find that PSELT exerts a strong neuroprotective effect both in cell culture and in animal models of PD, improving motor skill in the latter. We establish that PSELT is cell-permeable by itself and acts through an adaptive response including epigenetic control of gene expression, which contributes to efficient neuroprotection, thereby opening the way to a new therapy of PD.

2. Materials and Methods

2.1. Peptide synthesis

PSELT (H-Phe-Gln-Ile-Cys-Val-Ser-Sec-Gly-Tyr-Arg-OH) corresponding to amino acids 43–52 of SELENOT, the control peptide [$Ser^{46,49}$] PSELT, PSELT-dansyl and PSELT-TAT were synthesized by Fmoc solid phase methodology on a Liberty microwave assisted automated peptide synthesizer (CEM, Saclay, France) using the standard manufacturer's procedures at 0.1 mmol scale as previously described [31]. All Fmoc-amino acids were coupled *by in situ* activation with HBTU and DIEA, except for Sec which was coupled manually by *in situ* activation with HATU (0.2 mmol, 2 eq.), HOAt (0.2 mmol, 2 eq.) and DIEA (0.3 mmol, 3 eq.) in DMF during 90 min at room temperature. For the fluorescent peptide, the dansyl fluorochrome was coupled on the N-terminal part of PSELT using dansyl chloride (0.2 mmol, 2 eq) in DMF during 1 h at room temperature under light protection. After completion of the chain assembly, the peptides were deprotected, cleaved from the resin and purified by reversed-phase (RP) HPLC on a 21.2 × 250 mm Jupiter C18 (5 μm, 300 Å) column (Phenomenex, Le Pecq, France) using a linear gradient (10–40% over 45 min) of acetonitrile/TFA (99.9:0.1) at a flow rate of 10 ml/min. The purified peptides were then characterized by MALDI-TOF mass spectrometry on an UltrafleXtreme (Bruker, Strasbourg, France) in the reflector mode using α-cyano-4-hydroxycinnamic acid as a matrix. Analytical RP-HPLC, performed on a 4.6 × 250 mm Jupiter C18 (5 μm, 300 Å) column, indicated that the purity of the peptide was >99.9%.

2.2. Cell culture

The human SH-SY5Y neuroblastoma cell line (ATCC, Manassas, USA) was maintained in Dulbecco's modified Eagle's medium (Sigma-Aldrich, Saint-Quentin Fallavier, France), supplemented with 10% fetal bovine serum (Lonza, Levallois, France), 1% L-glutamine, 50 units/ml of penicillin and 50 units/ml of streptomycin (Thermo Fisher Scientific, Villebon-sur-Yvette, France), at 37 °C in 5% CO_2 humidified atmosphere. The medium was renewed every 2–3 days. Twenty-four hours after plating, cells were treated or not with 500 μM or 1 mM MPP^+ (Sigma-Aldrich) for 36 h in the presence or absence of PSELT (10 μM, dissolved in culture medium). The EZH2 inhibitor EPZ-6438 (Cliniciences, Nanterre, France), when present, was added at 10 μM at the same time as the peptide and MPP^+. For the microarray gene expression analysis, cells were treated with PSELT for 6 h only.

2.3. Cell viability assay

Cells were plated into 96-well plates (Corning, Wiesbaden, Germany) at 2×10^4 cells/well and subjected to MPP^+ and PSELT treatments. Cell viability was assessed using the CellTiter-Blue according to the manufacturer's instructions (Promega, Charbonnières les Bains, France). The fluorescence intensity (excitation at 544 nm and emission at 590 nm) was recorded using a Flexstation II spectrofluorophotometer (Molecular devices, Sunnyvale, USA).

2.4. Assessment of caspase-3-like activity

Caspase-3-like activity in cell culture was measured using the Apo-ONE Homogeneous Caspase-3/7 Assay Kit (Promega) according to the manufacturer's instructions. Briefly, cells in poly-L-lysine-coated 96-well plates (2×10^4 cells/well) were homogenized in the Homogeneous Caspase-3/7 buffer containing the caspase-3 substrate Z-DEVD-rhodamine 110, and the fluorescence intensity (excitation at 498 nm and emission at 521 nm) was measured in cell lysates during 3 h, using a Flexstation II spectrofluorophotometer (Molecular Devices).

2.5. Measurement of reactive oxygen species

SH-SY5Y cells cultured on coverslips in 12-well culture plates and the levels of intracellular ROS were measured using the DCFDA Cellular ROS Detection Assay Kit (Abcam, Cambridge, UK) following the manufacturer's instructions. The fluorescence of ROS-oxidized 2′,7′-dichlorofluorescein (DCF) was measured at 530 nm using a Flexstation II spectrofluorophotometer (Molecular devices).

2.6. RNA extraction and gene expression analysis

RNA was extracted using the TRIzol™ Reagent following the manufacturer's instructions (Sigma-Aldrich). Standard procedures for labeling, hybridization, washing and staining were as per manufacturer's recommendation (Affymetrix, Santa Clara, CA, USA). Briefly, the RNA was purified using a RiboPure Kit (Ambion, Austin, TX, USA) according to the manufacturer's protocol. The quality and quantity of RNA were ensured using the Bioanalyzer (Agilent, Santa Clara, CA, USA) and NanoDrop (Thermo Scientific, Waltham, MA, USA), respectively. For RNA labeling, total RNA (300 ng) was used in conjunction with the Affymetrix-recommended protocol with the WT Plus Reagent Kit. The hybridization cocktail containing the fragmented and labeled complementary DNAs (cDNAs) was hybridized to the Human GeneChip 2.0 ST chips. The chips were washed and stained by the Affymetrix Fluidics Station using the standard format and protocols from Affymetrix. The probe arrays were stained with streptavidin phycoerythrin solution (Molecular Probes, Carlsbad, CA, USA) and enhanced by using an antibody solution containing 0.5 mg/ml biotinylated *anti*-streptavidin (Vector Laboratories, Burlingame, CA, USA). The probe arrays were scanned using an Affymetrix Gene Chip Scanner 3000. Gene expression intensities were calculated using the Gene Chip Operating software 1.2 (Affymetrix). A GC-corrected robust multichip analysis (RMA) normalization model was used to correct for background, and nonspecific binding. All analyses were performed using Partek Genomics Suite. The raw data was submitted to Gene Expression Omnibus (GEO) under accession number GSE151808.

2.7. Dataset description and microarray data mining

Published microarray datasets in GEO (Gene Expression Omnibus) (http://www.ncbi.nlm.nih.gov/geo/) were mined to reveal phenotypes that may correlate with the present dataset using the broad institute Gene Set Enrichment Analysis program (GSEA) (http://broadinstitute.org/GSEA) according to the methods previously described [32–34]. Raw transcriptomic data was downloaded from the National Center for Biotechnology Information (NCBI) GEO database and imported into Partek Genomics Suite software (Partek, Inc., St. Louis, MI). After RMA normalization, log2 transformation and gene summarization, differentially expressed gene sets were generated based on ANOVA ($p < 0.05$ and 2-fold change). The GSEA algorithm computes a ranked list of all genes from our microarray and compare them to biologically well-defined and published gene signatures to determine whether individual genes of an a priori functionally defined gene set are enriched or randomly distributed across the whole ranked gene list, using a modified Kolmogorov-Smirnov statistic and generating an enrichment score. FDR q-value was set at $p < 0.05$, and statistical significance adjusted for multiple hypothesis testing was $p < 0.05$. A gene set-based permutation test of 1000 permutations was applied, and genes were ranked according to Student's t statistic. All other parameters were set to GSEA defaults.

Ingenuity Pathway Analysis (IPA) (http://www.ingenuity.com) (Ingenuity Systems, Redwood City, CA) was used to identify regulators associated with the differentially expressed genes.

2.8. Animals

All experimental procedures were approved by the Normandy Regional Ethics Committee (Authorization No. N/05-02-13/13/02–16) and were carried out in accordance with the European Committee Council Directive (2010-63-EU). Male C57BL/6J mice (24–27 g) or Wister rats (310–330 g) were housed under a 12-h light/12-h dark cycle (light on at 07:00 a.m.) and had free access to food and water. Ambient temperature was maintained at 22 °C ± 2 °C.

2.9. MPTP or 6-OHDA and peptide treatments

MPTP-HCl (Sigma-Aldrich) was dissolved in sterile 0.9% saline and intraperitoneally injected to 12-week-old male C57BL/6J mice. MPTP at 30 mg/kg was injected daily during five days. Control animals were intraperitoneally injected with sterile 0.9% saline. Mice received intranasal administration of 30 μg of PSELT per animal in 10 μl saline (5 μl per nostril) for 6 days, while control animals received saline only. After the different treatments, the animals were anesthetized with sodium pentobarbital (120 mg/kg; Ceva Santé Animale, Libourne, France), heparinized and perfused through an intracardiac cannula with 0.9% NaCl in 0.1 M phosphate buffer (pH 7.4), followed by 4% paraformaldehyde (PFA) in PBS. Brains were removed and post-fixed in the same fixative at 4 °C during 24 h. Then, brains were conserved at 4 °C in PBS azide.

In the 6-OHDA model, animals were anesthetized with 4% chloral hydrate (Sigma-Aldrich, Paris, France) (300 mg/kg, i.p.) and mounted in a stereotactic apparatus. Free base 6-OHDA hydrochloride (8 μg; Sigma-Aldrich) was dissolved, immediately before use, in 4 μl saline containing 0.01% ascorbic acid and injected into the SNc at the following stereotaxic coordinates: AP: 5.3 mm posterior to bregma, L: 2.3 mm from the midline, D: 7.0–7.3 mm from the dura. The injection was made at a rate of 0.5 μl/min using a cannula connected by polyethylene tubing to a 25 μl Hamilton microsyringe and driven by an infusion pump. At the end of each injection the syringe needle was left in place for an additional 10 min and then withdrawn slowly to prevent reflux of the solution. PSELT was administered daily also by stereotaxis in the SNc at 1 μM in 2 μl during 8 days, and the animals were sacrificed 7 days later. Brains were then collected as described above.

2.10. Immunofluorescence

Fixed tissues were sectioned into 40-μm slices with a vibratome. The sections were incubated with 1% donkey serum diluted in 1% bovine serum albumin and 0.3% Triton X-100 in PBS for 2 h at room temperature, and then exposed overnight at 4 °C to primary antibodies, including anti-TH diluted 1:200 (Millipore, Guyancourt, France), anti-TAT diluted 1:200 (Sigma-Aldrich), *anti*-EZH2 diluted 1:200 (Ozyme, Saint-Cyr-l'école, France), or anti-active caspase 3 (Cell Signaling, Danvers, USA) diluted 1:400. Immunostaining was visualized using Alexa Fluor 488 or 594 conjugated secondary antibodies diluted 1:200 (Invitrogen, Saint Aubin, France). Nuclei were stained with 1 μg/ml 4,6-diamino-2-phenylindole (DAPI, Sigma-Aldrich) or 1 μM TO-PRO3 in PBS prior to mounting the slides with PBS/glycerol 50/50. Samples were analyzed with a Leica TCS SP8 confocal microscope (Leica Microsystems, Nanterre, France).

2.11. Western blot analysis

Animals were anesthetized by isoflurane inhalation, and the brains were immediately recovered after decapitation and quickly placed in dry ice. Tissue and cell samples were homogenized in a lysis buffer (Ozyme, Saint-Quentin-en-Yvelines, France) or RIPA buffer (Sigma-Aldrich) and analyzed by electrophoresis and protein transfer onto a PVDF membrane (Thermo Fisher Scientific). For all experiments, 30 μg of proteins was used. Membranes were probed with polyclonal antibodies against TH (Millipore) diluted 1:200, anti-active caspase 3 diluted 1:200 (Cell Signaling, Danvers, USA), phosphoTH-Ser31 diluted 1:500, phosphoTH-Ser40 (Ozyme) diluted 1:400, BiP/GRP78 (Sigma-Aldrich) diluted 1:100, DJ-1/PARK7 (Millipore) diluted 1:100, α-synuclein (Sigma-Aldrich) diluted 1:250, *anti*-H3K27me diluted 1:500 (Diagenode, Ougrée, Belgium) and *anti*-H3 diluted 1:500 (Abcam). After incubation with Alexia conjugated secondary antibodies (Thermo Fisher Scientific) diluted at 1:1000, the resulting immune complexes were visualized using the ECL chemiluminescence system (Thermo Fischer Scientific). An antibody against α-tubulin (Sigma-Aldrich) or GAPDH (Sigma-Aldrich) diluted at 1:1000, was used as a control to ensure equal protein loading.

2.12. Dopamine assay

Dopamine concentrations in striatum homogenates from the different animal groups were determined using a mouse dopamine Elisa kit following the manufacturer's instructions (Mybiosource, San Diego, CA).

2.13. Behavioral tests

2.13.1. Open-field locomotor activity

Locomotor activity was assessed automatically in a computerized actimeter (Versamax, AccuScan Instruments, Inc., Ohio, USA) which monitored horizontal displacements and vertical movements, including rearing, leaning and jumping. The animals were placed individually in 20 × 20 × 30 cm compartments in a dimly illuminated and quiet room. The activities were measured during three consecutive periods of 10 min each.

2.13.2. Rotarod

The Rotamex-5 (Columbus Instruments, OH, USA) was used for the evaluation of motor coordination. Mice were placed onto the rod of the apparatus. Rotation was started at 2 rpm to allow the mice to balance and then increased by about 0.4 rpm/s, up to a maximum of 10 rpm. The latency at which the mice were able to maintain their balance on the bar was then recorded automatically by Columbus instruments Rotamex software, using photobeam break technology. The average latency of the last two trials in each day was used for analyses.

2.14. MALDI-TOF mass spectrometry

Brain extracts or cell lysates were pre-purified using SEP-PAK C18 cartridges (Waters Associates, Milford, MA). Before adding the samples, the cartridges were conditioned in 100% of acetonitrile followed by 0.12% trifluoroacetic acid in water. The elution was carried out using a gradient of acetonitrile. The fraction eluted at 50% was recovered for analysis by MALDI-TOF mass spectrometry. Eluates were analyzed by MALDI-TOF mass spectrometry on an UltrafleXtreme (Bruker, Strasbourg, France) operating in positive reflector mode. Spectra were recorded using α-cyano-4-hydroxycinnamic acid as a matrix. The instrument was calibrated with peptides of known molecular mass in the 1–2 kDa range.

2.15. Statistics

Results are expressed as mean ± SEM and represent data from a minimum of three independent experiments *in vitro* or from groups of 5-12 animals. Statistical analysis of the data was performed with GraphPad Prism 6 software. Statistical significance of difference between groups was determined by the Student's *t*-test or after one-way ANOVA with Tukey's multiple comparisons test.

3. Results

3.1. PSELT protects dopaminergic cells by inhibiting MPP^+-induced ROS production

To test the potential protective effect of PSELT in neurotoxic conditions, we first used the neuroblastoma cell line SH-SY5Y as a model of dopaminergic neurons where degeneration can be induced in the presence of 1-methyl-4-phenylpyridinium (MPP^+), the active form of the dopamine system-targeting neurotoxin 1-methyl-4-phenyl-1,2,3,6-tetrahydropyridine (MPTP). MPP^+ acts on mitochondrial complex I and induces massive oxidative stress *in vitro* and *in vivo*. We found that PSELT at 1 μM is able to promote neuroblastoma cell survival against MPP^+ (1 mM) toxicity (Fig. 1A and B). A dose-response curve revealed that PSELT is maximally effective at 1 μM (Fig. 1C). When a control peptide ([$Ser^{46,49}$]PSELT), where the Sec and the Cys residues of PSELT were replaced by isosteric Ser moieties was used, no protective effect was observed (Fig. 1D), indicating that PSELT exerts its protective action most likely through a redox mechanism involving the formation of a selenyl-sulfide bridge. The pro-survival effect of PSELT was confirmed by its inhibitory effect on MPP^+-induced caspase 3/7 activity (Fig. 1E). To determine whether PSELT could control the oxidative stress provoked by MPP^+ treatment, we used the DCF probe whose intracellular fluorescence reflects free radical levels. The results showed that PSELT treatment significantly reduces ROS levels generated in the presence of MPP^+ (Fig. 1F), indicating that PSELT is able to counteract oxidative stress and to impact redox regulation in order to protect dopaminergic cells.

3.2. PSELT is cell-permeable

To gain insight into the mechanism of action of PSELT, we wished to determine if its effects occur at different cellular compartments and if so, do these effects occur at sites of action within the cell, or possibly via actions initiated at the plasma membrane from the extracellular space. We first compared the effect of PSELT to that of PSELT attached to a TAT cell-penetrating peptide, which revealed that the TAT peptide does not modify or improve the effect of PSELT since the two peptide forms were equally effective in promoting neuroblastoma cell survival (Fig. 2A). We then asked whether PSELT could affect the expression of proteins associated with different biological processes linked to PD and located in different cell compartments. For this purpose, we measured the effect of PSELT on the expression of the cytoplasmic protein α-synuclein which is mutated in PD, the ER protein glucose-regulated protein 78 (GRP78/BiP) which is deregulated in PD and the nuclear protein histone 3 lysine 27 trimethylated mark (H3K27me3) which is associated with epigenetic alterations in the disease. This analysis revealed that PSELT is able to decrease α-synuclein (Fig. 2B and C) and GRP78 (Fig. 2D and E) levels, and to increase H3K27me3 levels (Fig. 2F and G), indicating that the peptide is able to trigger a multi-level action and to regulate different intracellular events associated with dopaminergic cell function. In addition, the fact that PSELT up-regulates H3K27me3 level suggests that the peptide action would involve epigenetic regulation.

We next generated a fluorescent form of PSELT by coupling a dansyl fluorophore to the N-terminus of the peptide (PSELT-dansyl) in order to examine its distribution after incubation with cultured SH-SY5Y cells. After 5 min of incubation, we could visualize by confocal microscopy

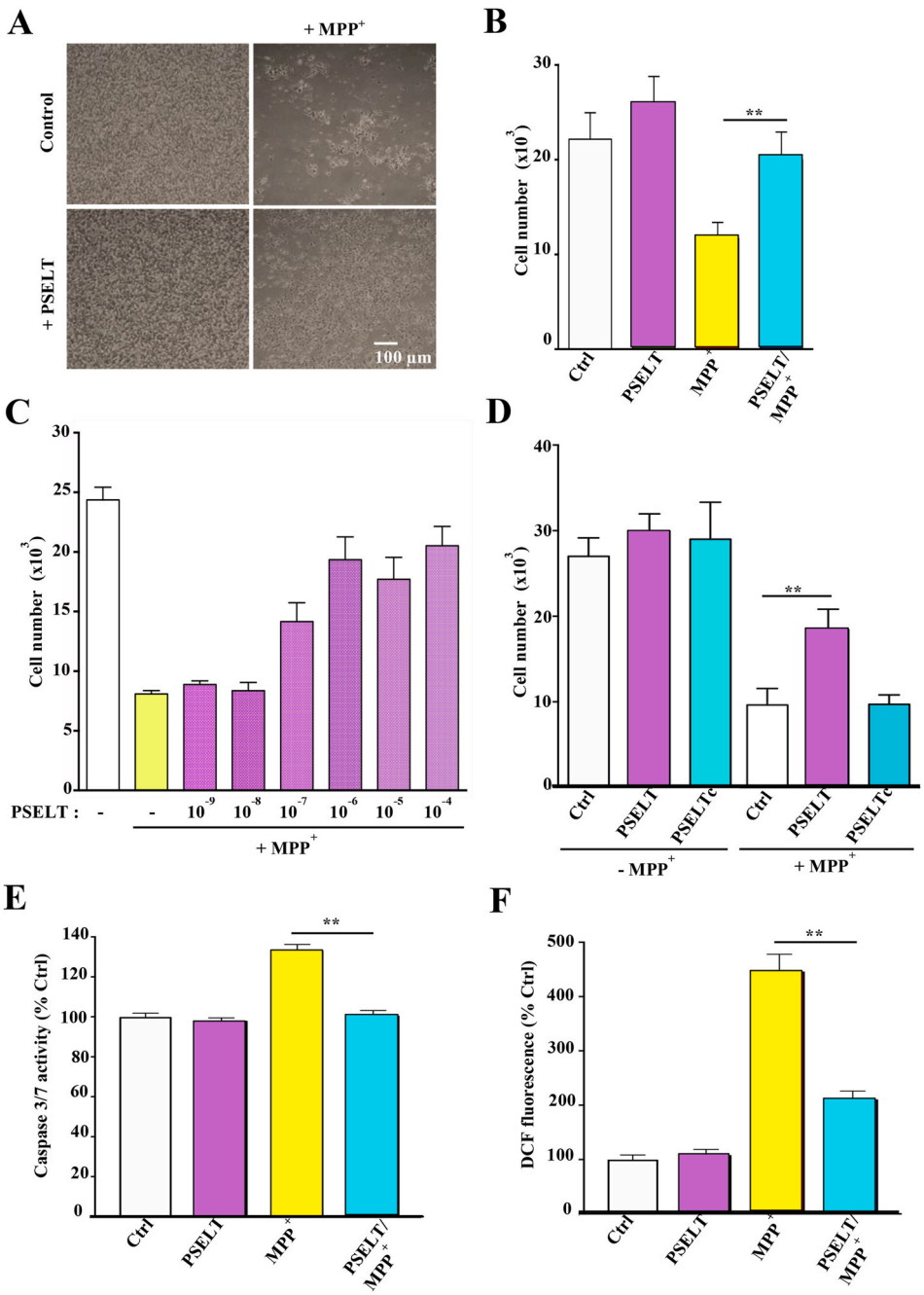

Fig. 1. PSELT, and not a control peptide, protects SH-SY5Y cells.
A: Photomicrographs of SH-SY5Y cells treated or not with MPP^+ (1 mM) in the presence or absence of PSELT (1 μM) for 36 h. Scale bar: 100 μm
B: Quantification of cell numbers in the different conditions indicated in (A). Data are expressed as mean ± SEM and are compared using Student *t*-test, $^{**}p < 0.01$ ($n = 3$ per condition).
C: PSELT dose-response effect on cell survival. Cell number was determined after treatment with MPP^+ (1 mM) in the presence or absence of the indicated concentrations of PSELT for 36 h. Data are expressed as mean ± SEM ($n = 4$ per condition).
D: Cell number was quantified after treatment with or without PSELT or a control PSELT (PSELTc) where the Sec was replaced by a Ser residue (1 μM), in the presence or absence of MPP^+ (1 mM) for 36 h. Data are expressed as mean ± SEM and are compared using Student *t*-test, $^{**}p < 0.01$ ($n = 3$ per condition).
E: Caspase 3/7 activity was assessed as described in Materials and Methods, in the different conditions indicated in (A). Data are expressed as mean ± SEM and are compared using Student *t*-test, $^{**}p < 0.01$ ($n = 3$ per condition).
F: Free radicals were quantified through DCF fluorescence as described in Materials and Methods in the different conditions indicated in (A), and the data were presented as mean ± SEM and compared using Student *t*-test, $^{**}p < 0.01$ ($n = 3$ per condition).

several PSELT-dansyl fluorescent dots within the cells (Fig. 3A). After 15 min of incubation, the labeling was more intense in the cytoplasm and exhibited an ER-like shape (Fig. 3A). Several fluorescent dots were also observed in the nuclei at this time of incubation (Fig. 3A). At 6 h of incubation, the fluorescent peptide was still observed in the cytoplasm and the nuclei, and also in the nucleoli (Fig. 3A). In order to confirm the penetration of the peptide *per se* (without dansyl) into the cells, we performed mass spectrometry analysis of extracts from cells incubated with and without the free PSELT for different times, and compared the mass spectrum profiles obtained to the mass profile of the peptide analyzed separately (Fig. 3B–E). At all times examined, this analysis revealed the presence in the cell extracts of a PSELT mass spectrometry pattern comparable to that observed for the free peptide analyzed alone, with similar mass and isotopic profiles (Fig. 3B–E), supporting the previous confocal microscopy results and demonstrating that PSELT is able to cross the biological membranes and is thus cell-permeable. Of note, PSELT was still detected in the cells after 48 h of incubation (Fig. 3E). As expected, control cells which were not incubated with the peptide did not show the PSELT mass profile (Fig. 3F). Together, these data revealed that PSELT has the capacity to penetrate cells and to reach several intracellular organelles, where it can affect different targets.

3.3. *Intranasal delivery of PSELT to the nigrostriatal pathway in mice*

To determine whether PSELT can be targeted to the nigrostriatal dopaminergic system *in vivo*, we used the intranasal route to deliver PSELT into the brain and to assess its destination to dopaminergic neurons and fibers of the SNc and striatum (Str), respectively. In order to detect PSELT in the brain after intranasal administration, we used PSELT combined with the TAT peptide, for which an antibody was available and could be employed to localize PSELT in the dopaminergic pathway, which was labeled with antibodies against tyrosine hydroxylase (TH).

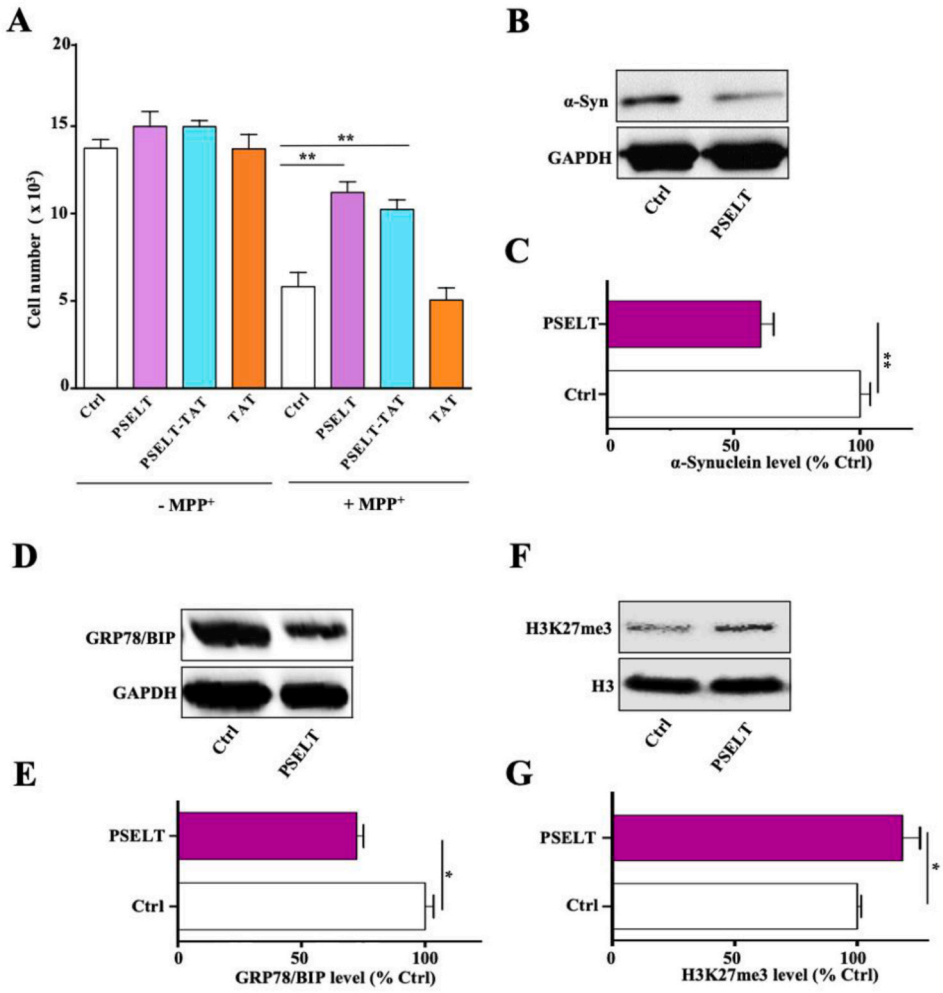

Fig. 2. PSELT effects in SY5Y cells.
A: Cell number was quantified after treatment with or without PSELT, PSELT-TAT or TAT alone (1 μM), in the presence or absence of MPP^+ (1 mM) for 36 h. Data are expressed as mean ± SEM and are compared using ANOVA and Tukey's test, $^{**}p < 0.01$ ($n = 3$ per condition).
B: Alpha-synuclein (α-Syn) was examined by Western blot in control or PSELT-treated cells and normalized to GAPDH levels.
C: Quantification of α-Syn levels from (B). Data are expressed as mean ± SEM and are compared using Student *t*-test, $^{**}p < 0.01$ ($n = 3$ per condition).
D: Glucose-regulated protein (GRP78) was examined by Western blot in control or PSELT-treated cells and normalized to GAPDH levels.
E: Quantification of GRP78/BIP levels from (D). Data are expressed as mean ± SEM and are compared using Student *t*-test, $^{*}p < 0.05$ ($n = 3$ per condition)
F: The methylation mark H3K27me3 was examined by Western blot in control or PSELT-treated cells and normalized to histone H3 levels.
G: Quantification of H3K27me3 levels from (F). Data are expressed as mean ± SEM and are compared using Student *t*-test, $^{*}p < 0.05$ ($n = 3$ per condition). The data shown are representative of at least 2–3 experiments with similar results.

Two hours after intranasal administration, the peptide-TAT signal exhibited a diffuse localization in the SNc area and a strong intensity in the Str (Fig. 4A and B). After 4 h, the immunofluorescent PSELT-TAT signal was more concentrated in the dopaminergic neurons of the SNc (Fig. 4, A and C) and in dopaminergic fibers along with other cells in the Str (Fig. 4B and C). Higher magnification revealed that PSELT-TAT immunofluorescence is localized inside the cells including the nuclei (Fig. 4C), as was observed in neuroblastoma cells in culture (Fig. 3). To confirm the presence of the free PSELT peptide in the dopaminergic system *in vivo*, we analyzed, by mass spectrometry, PSELT occurrence in the Str after its intranasal administration. This experiment revealed that free PSELT is indeed present in the Str *in vivo* after intranasal administration (Fig. 4D). Together, these data showed that PSELT is able to reach and accumulate in dopaminergic cells and fibers of the nigrostriatal pathway within few hours after its intranasal administration.

3.4. PSELT protects the dopaminergic system in vivo

In order to test its potential protective effect *in vivo*, PSELT was administered daily through the intranasal route (30 μg/10 μl) to mice that were treated in parallel with MPTP (30 mg/kg) intraperitoneally for 5 days. Immunohistochemical labeling of TH showed that MPTP provokes a marked degeneration of dopaminergic neurons in the SNc (Fig. 5A) and dopaminergic fibers in the Str (Fig. 5B), which was largely prevented by PSELT (Fig. 5A and B). This result was confirmed by assessing active caspase 3 immunoreactivity whose MPTP-induced increase was prevented by PSELT (Fig. 5A and B). Western blot analysis revealed that PSELT is able to significantly attenuate the MPTP-induced decrease of TH levels (Fig. 5C and D) and the MPTP-induced increase in active caspase-3 levels (Fig. 5, C and E). Interestingly, PSELT was also able to attenuate the MPTP-induced decrease in DJ-1 levels (Fig. 5, C and F), a protein implicated in the control of oxidative stress in PD [35]. In addition, PSELT also reversed the MPTP-induced decrease in Ser^{31}- and Ser^{40}-phosphorylated TH, the active forms of the enzyme (Fig. 5G–I). Finally, PSELT showed a clear tendency to preserve dopamine levels in the Str measured at day 7 post-treatment, but the difference between the PSELT/MPTP- and MPTP-treated groups did not reach statistical significance (Fig. 5J).

Next, we sought to further demonstrate efficacy of PSELT action using a second PD rodent model based on stereotactic administration of the neurotoxin 6-hydroxydopamine (6-OHDA) in the rat nigral pathway. In this other model of PD, PSELT administered stereotactically along with 6-OHDA also protected both the SNc and the Str against 6-OHDA-induced degeneration as revealed by TH and caspase 3 immunolabelings and their quantification (Fig. 6A–D). Western blot analysis confirmed the protective effect of PSELT against 6-OHDA-triggered neurodegeneration in the rat nigral pathway as assessed by TH quantification in the Str (Fig. 6E and F).

3.5. Molecular effects and pathways associated with PSELT action in dopaminergic cells

To define PSELT molecular and functional impact more globally, we performed a transcriptomic analysis of SH-SY5Y cells after treatment

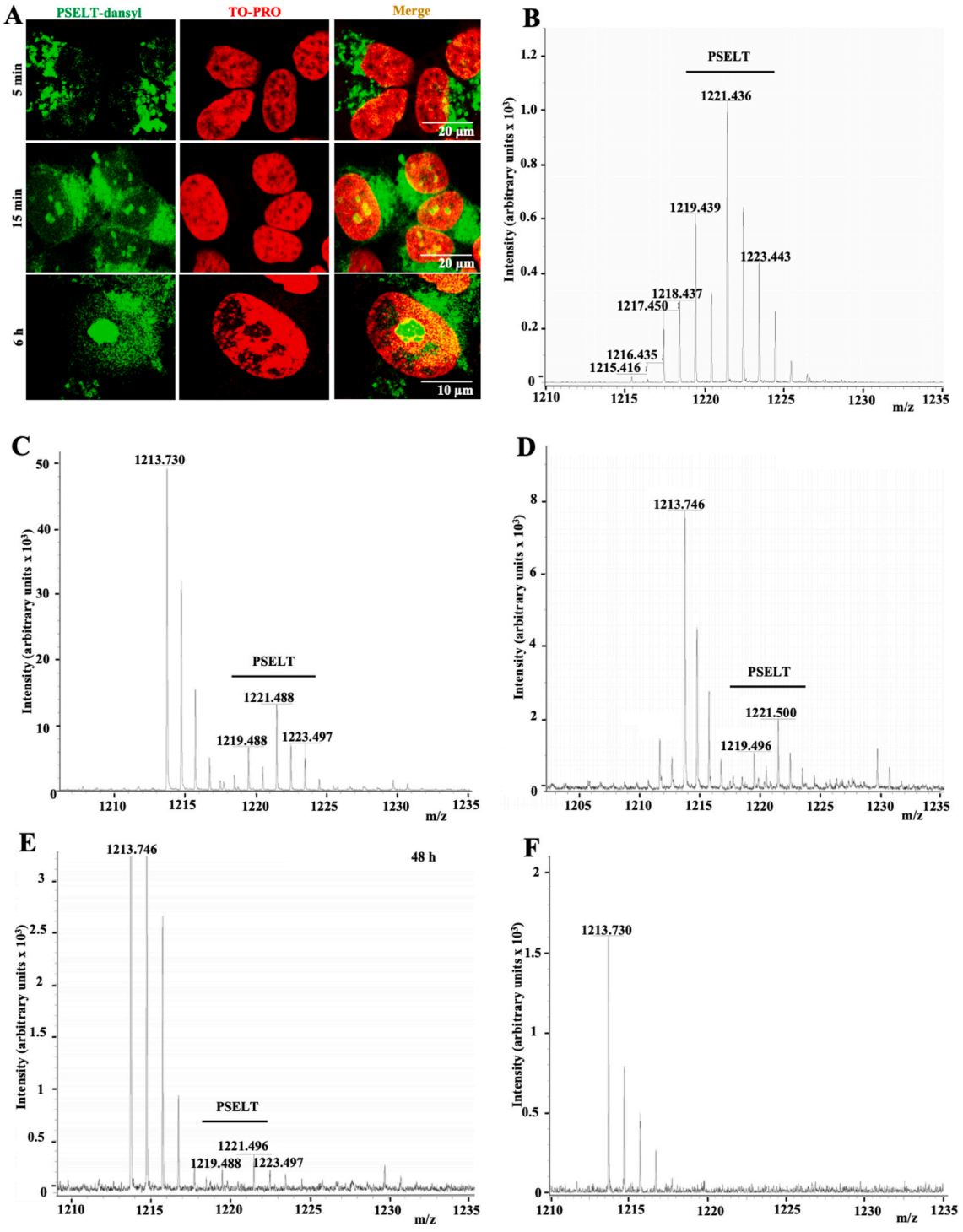

Fig. 3. PSELT reaches intracellular compartments.
A: Confocal microscopic images of SH-SY5Y cells that were incubated for 5 min, 15 min and 6 h in the presence of PSELT labeled by the fluorochrome dansyl. The nuclei were stained by the TO-PRO3 dye. Scale bars: 10 and 20 µm.
B: Mass spectrometric profile of PSELT alone showing several pics due to the existence of different selenium isotopes.
C: Mass spectrometry analysis of SH-SY5Y cell extracts after incubation of the cells with PSELT for 30 min.
D: Mass spectrometry analysis of SH-SY5Y cell extracts after incubation of the cells with PSELT for 1 h
E: Mass spectrometry analysis of SH-SY5Y cell extracts after incubation of the cells with PSELT for 48 h.
F: Mass spectrometry analysis of a control SH-SY5Y cell extract without PSELT incubation. No peak was seen in the PSELT mass position.

with MPP^+ (1 mM) in the presence or absence of PSELT (1 µM) for 6 h. The transcriptomic response to treatment with MPP^+ was strongly affected by co-administration of PSELT as revealed by microarray data analysis. An unsupervised hierarchical clustering of the top 500 differentially expressed genes (P value < 0.05) revealed that PSELT is able to reverse the expression of genes up- or down-regulated by MPP^+ as shown in Fig. 7A, indicating that PSELT protection of dopaminergic neurons extends globally to reversal of transcriptomic changes

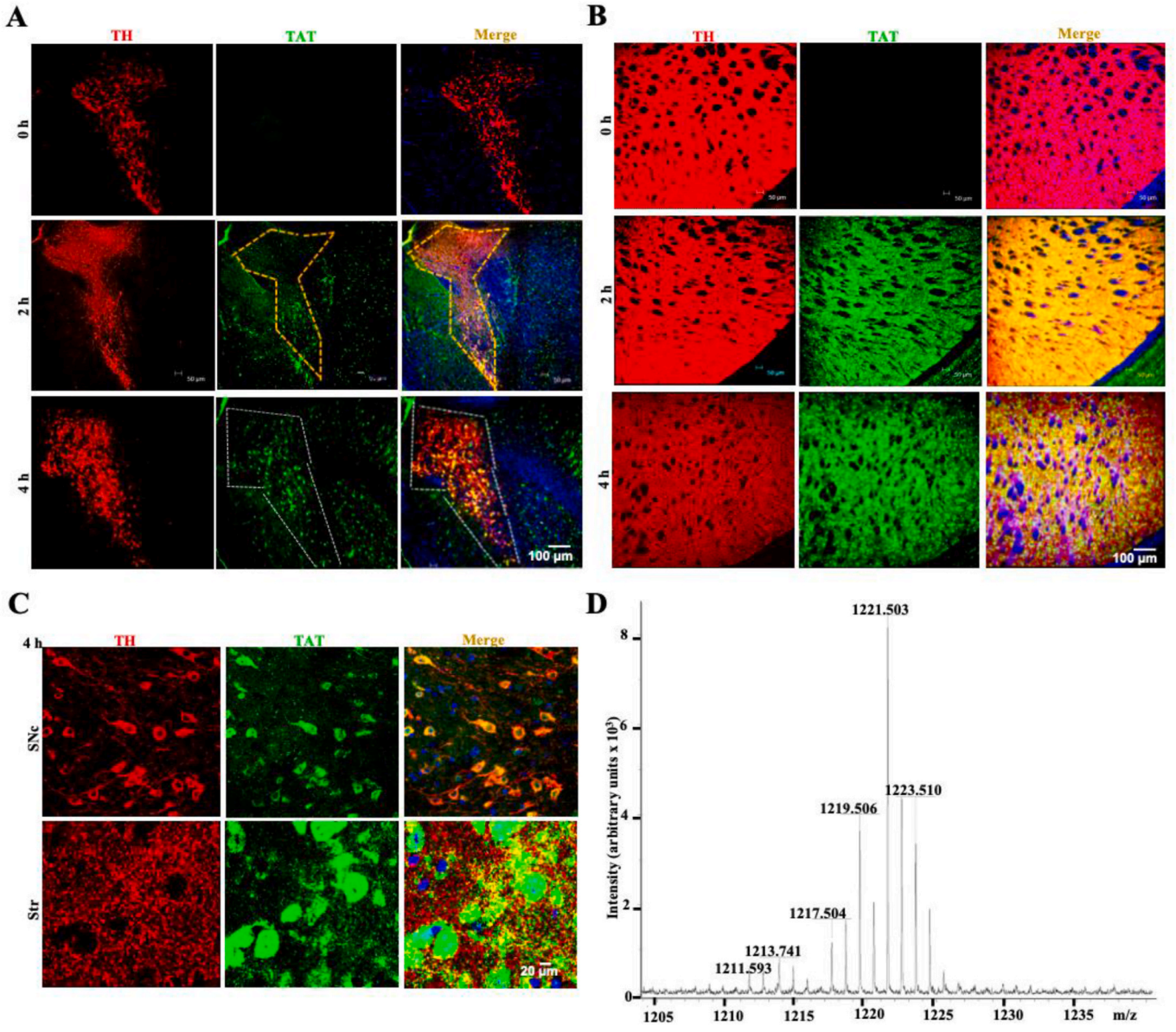

Fig. 4. Intranasal delivery of PSELT to the nigrostriatal pathway.

A: TH and TAT immunostaining was performed in the SNc after intranasal administration of PSELT-TAT, at 2 and 4 h post-treatment. Note that there is no PSELT-TAT signal in control nigral tissue while a strong signal was detected at 4 h in this area (dashed). Nuclei were stained in blue with DAPI. Scale bar: 100 µm.

B: TH and TAT immunostaining was performed in the Str after intranasal administration of PSELT-TAT, at 2 and 4 h post-treatment. Note that there is no PSELT-TAT signal in control striatal tissue while a strong signal was detected at 2 and 4 h in this area. Nuclei were stained in blue with DAPI. Scale bar: 100 µm.

C: Higher magnification in the SNc and Str areas 4 h after intranasal administration of PSELT showing that the peptide is present in dopaminergic neurons and fibers and reaches the nuclei. Scale bar: 20 µm.

D: Mass spectrometry analysis of a striatal extract after intranasal administration of PSELT for 5 consecutive days as described in the present study in PD models (see below). (For interpretation of the references to color in this figure legend, the reader is referred to the Web version of this article.)

indicative of oxidative distress accompanying neurodegeneration elicited by MPP^+ in these cells. Using gene set enrichment analysis (GSEA) with all genes for the comparison of MPP^+ and MPP^++PSELT conditions, we found that genes up-regulated by MPP^+ and down-regulated by PSELT are also up-regulated in PD as described in a study reported by Dumitriu et *al.* [36] who profiled 29 PD patients and compared them to 44 neurologically normal controls (Fig. 7B and Fig. S1A for more correlative analyses with PD gene sets). Similarly, genes down-regulated in gene sets associated with neurogenesis and aging/caloric restriction pathways were correlated to genes down-regulated by MPP^+ and up-regulated by PSELT (Fig. 7C and D, and Fig. S1B for more correlative analyses with neurogenesis gene sets). The gene set most highly correlated with PSELT action is the one for treatment with the antioxidant and anti-inflammatory compound resveratrol [37] (Fig. 7E and Fig. S1C for more correlative analyses with resveratrol-regulated gene sets). For instance, genes that were described as down-regulated by resveratrol in peripheral blood mononuclear cells were also down-regulated by PSELT in neuroblastoma cells and reciprocally, genes up-regulated by resveratrol are also up-regulated by PSELT (Fig. 7E).

In a search of a master gene whose dysregulation by oxidative distress might trigger a widespread transcriptional response mitigated by treatment with PSELT, we found that genes described in the NCBI database as associated/interacting with the EZH2 protein, a master transcription regulator acting epigenetically, are significantly correlated with PSELT treatment (Fig. 7F and Fig. S1D for more correlative analyses), and that genes up-regulated after EZH2 knockout with a

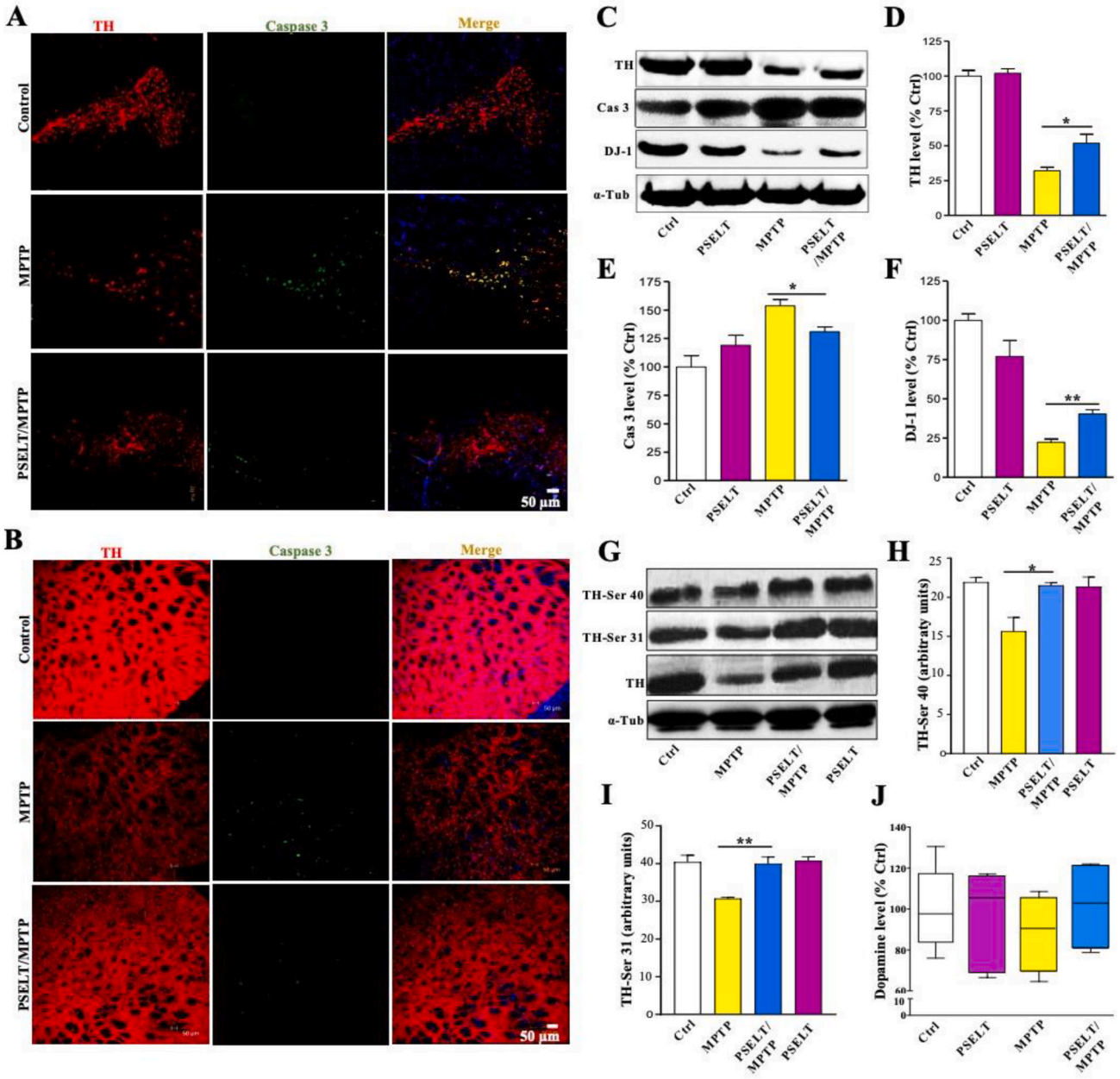

Fig. 5. PSELT protects the nigrostriatal dopaminergic pathway against MPTP insult.

A: Exposure to MPTP provoked the degeneration of dopaminergic neurons in the SNc as revealed by TH and caspase 3 immunolabelings of tissue sections at 7 days post-treatment. Scale bar: 50 µm

B: Exposure to MPTP provoked a degeneration of dopaminergic fibers in the Str as revealed by TH and caspase 3 immunolabelings of tissue sections at 7 days post-treatment. Scale bar: 50 µm.

C: Western blot analysis of TH, caspase 3 and DJ-1 levels in the striatum of control and MPTP-treated mice in the presence or absence of PSELT. Alpha-tubulin was used as a protein loading control to normalize the data.

D: Quantification of TH level after Western blot analysis of striatal samples from control and MPTP-treated animals in the presence or absence of PSELT ($*p < 0.05$; $n = 10$).

E: Quantification of caspase 3 level after Western blot analysis of striatal samples from control and MPTP-treated animals in the presence or absence of PSELT ($*p < 0.05$; $n = 10$)

F: Quantification of DJ-1 level after Western blot analysis of striatal samples from control and MPTP-treated animals in the presence or absence of PSELT ($**p < 0.01$; $n = 10$).

G: Western blot analysis of TH-Ser 40, TH-Ser 31 and TH levels levels in the striatum of control and MPTP-treated mice in the presence or absence of PSELT. Alpha-tubulin was used as a protein loading control to normalize the data.

H: Quantification of TH-Ser 40 level after Western blot analysis of striatal samples from control and MPTP-treated animals in the presence or absence of PSELT ($*p < 0.05$; $n = 10$)

I: Quantification of TH-Ser 31 level after Western blot analysis of striatal samples from control and MPTP-treated animals in the presence or absence of PSELT ($*p < 0.01$; $n = 10$).

J: Striatal dopamine level of control and MPTP-treated animals in the presence or absence of PSELT ($n = 5$). This experiment was repeated 3 times with similar results.

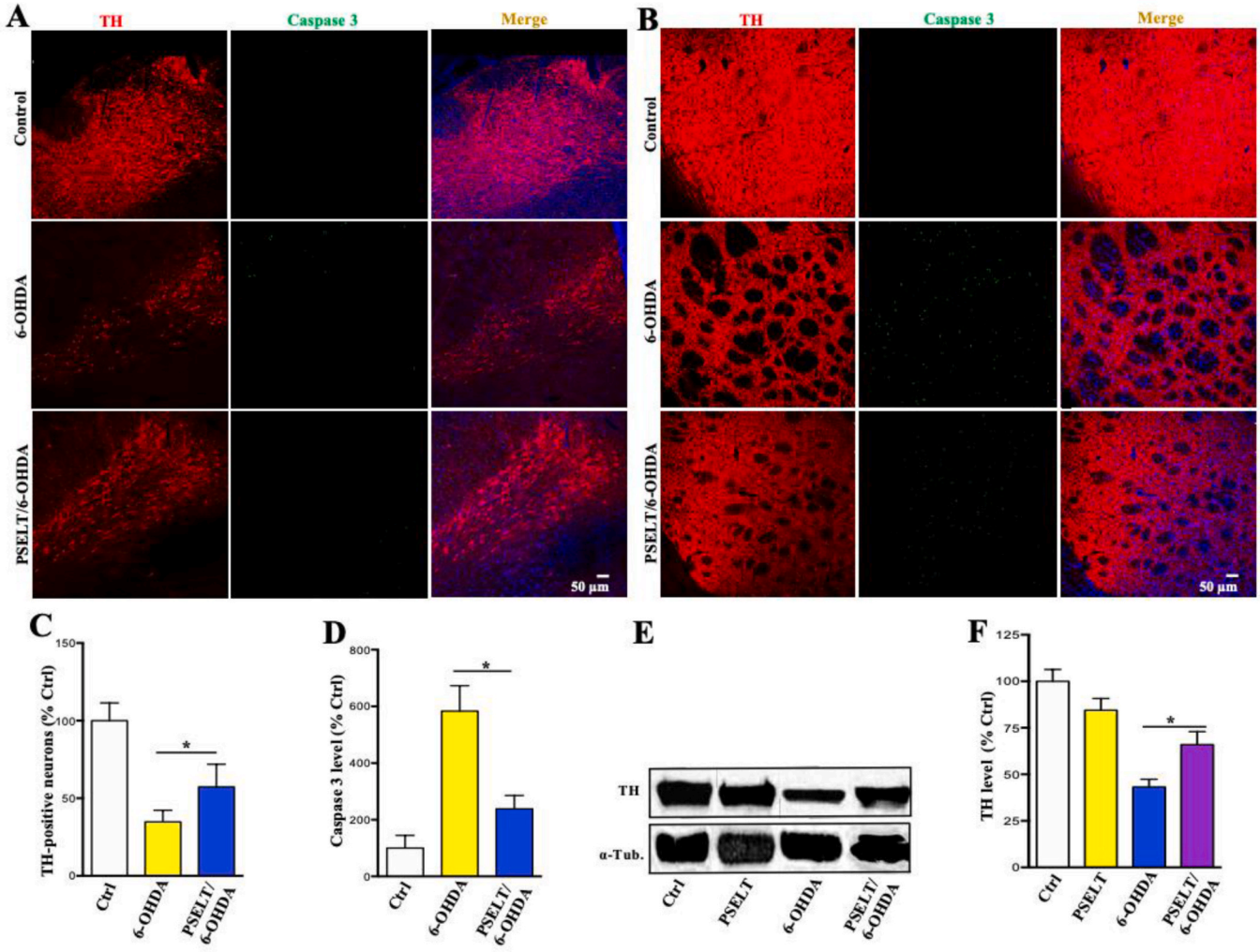

Fig. 6. PSELT protects the nigrostriatal dopaminergic pathway in 6-OHDA-treated rats.
A: Stereotactic administration of 6-OHDA provoked the degeneration of dopaminergic neurons in the SNc as revealed by TH and caspase 3 immunolabelings of tissue sections 2 weeks after 6-OHDA treatment. PSELT (1 μM) administration during the first week attenuated the neurodegeneration. Scale bar: 50 μm.
B: Stereotaxic administration of 6-OHDA also provoked the degeneration of dopaminergic fibers in the Str as revealed by TH and caspase 3 immunolabelings of tissue sections 2 weeks after 6-OHDA treatment. PSELT (1 μM) administration during the first week attenuated the neurodegeneration. Scale bar: 50 μm.
C: Quantification of TH-positive neurons after 6-OHDA treatment in the presence or absence of PSELT. Data are expressed as mean ± SEM and are compared using Student *t*-test, $*p < 0.05$ ($n = 5$)
D: Quantification of caspase 3 immunoreactivity in the SNc from control and 6-OHDA-treated animals in the presence or absence of PSELT ($*p < 0.05$; $n = 5$).
E: Western blot analysis of TH levels in the str of control and 6-OHDA-treated rats in the presence or absence of PSELT. Alpha-tubulin was used as a protein loading control to normalize the data.
F: Quantification of TH level after Western blot analysis of striatal samples from control and 6-OHDA-treated animals in the presence or absence of PSELT ($*p < 0.05$; $n = 5$).

H3K27me3 mark [38] correlate with genes up-regulated by MPP^+ and down-regulated by PSELT (Fig. 7G). These gene expression correlation analyses support the notion that PSELT may promote redox homeostasis and cell survival through epigenetic regulation.

3.6. *PSELT regulates EZH2/H3K27 expression to promote cell survival*

In order to test the possibility that PSELT could act at the epigenetic level, *i.e.* alteration of EZH2 expression, that would explain at least in part the large transcriptomic effects observed, we focused on this pathway by analyzing first the effect and colocalization of PSELT and EZH2 in neuroblastoma cells. Although EZH2 was barely detectable by immunohistochemistry in these cells in control conditions, its levels were markedly increased in the nuclei after 15 min and 6 h of treatment with PSELT (Fig. 8A and B). At both times, PSELT and EZH2 colocalized in the nuclei which were labeled by the TO-PRO dye (Fig. 8A). Since EZH2 is responsible for the trimethylation of the histone H3K27 [39], we sought to determine whether PSELT also affects the levels of H3K27me3 mark in neuroblastoma cells. Western blot analysis showed that PSELT also increased the levels of H3K27me3 and this effect was abolished by EPZ6438, a selective inhibitor of EZH2 activity (Fig. 8C and D). Moreover, the H3K27me3 mark was repressed by MPP^+, but EZH2 inhibitor had no significant effect on the level of the methylation mark in this condition (Fig. 8C and D), suggesting that MPP^+ and EZH2 inhibitor both act on EZH2 to inhibit H3K27me3 levels. In the presence of MPP^+, PSELT no longer stimulated the histone methylation mark, whose level was further reduced by EZH2 inhibitor (Fig. 8C and D). These results indicate that PSELT exerts epigenetic effects in SH-SY5Y cells through EZH2 and H3K27me3 regulation. To determine whether PSELT-induced effect on EZH2/H3K27me3 levels is involved in cell survival, we measured cell viability under MPP^+/PSELT treatment in the absence or presence of EPZ6438. Cell viability measurements revealed that EZH2

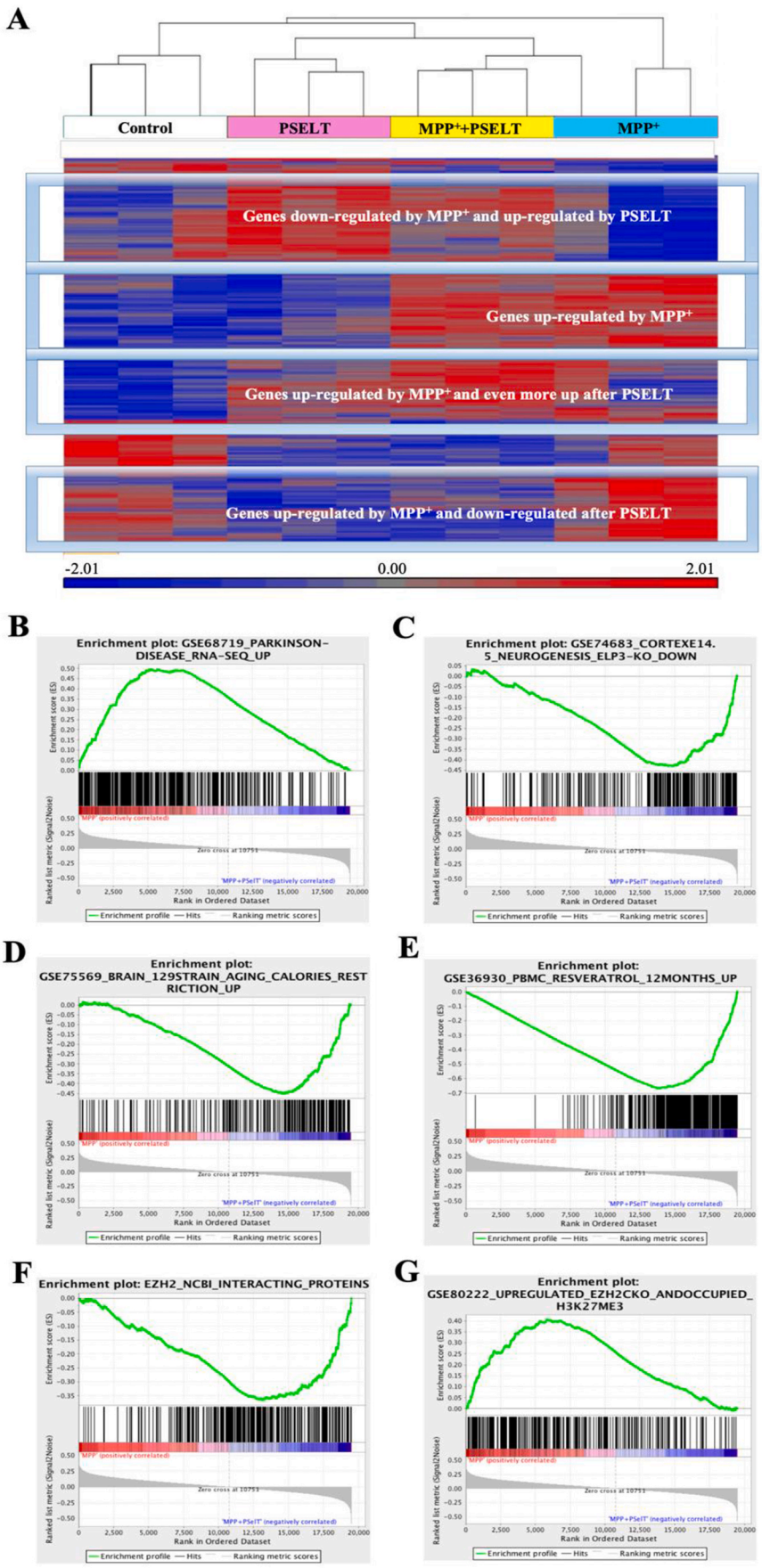

Fig. 7. PSELT effect on gene expression levels in SH-SY5Y cells correlates with different gene sets.

A: Unsupervised clustering based on gene expression profiling of the different experimental conditions indicated under the dendrogram ($n = 3$ per condition). Genes with a relatively higher level of expression are shown in red, and those with a lower level are shown in blue according to the color scale at the bottom.

B: Gene set enrichment analysis of a ranked list of all genes comparing MPP^+ and PSELT treatment versus MPP^+ with those up-regulated in Parkinson's disease (p value = 0, enrichment score = 1.15). Genes up-regulated in Parkinson's disease positively correlate with genes up-regulated by MPP^+ and down-regulated by PSELT. Data were taken from GSE68719_Parkinson disease [36] or from GSE78757_Gaucher disease, GSE20292_Parkinson substantia nigra and GSE9397_Parkinson MSN [36,61,62] in supplementary Fig.S1A.

C: Gene set enrichment analysis of a ranked list of all genes comparing MPP^+ and PSELT treatment versus MPP^+ with those down-regulated in cortical neurogenesis (p value = 0, enrichment score = −1.29). Genes down-regulated during impaired corticogenesis correlate with genes up-regulated by PSELT. Data were taken from GSE74683_Cortex_Neurogenesis (ELP3 knockout) [63] or from GSE 42904_HIPPO [64], GSE8425_RASGRF1 KO [65] and the orphan nuclear receptor TLX targets [66] in supplementary Fig.S1B.

D: Gene set enrichment analysis of a ranked list of all genes comparing MPP^+ and PSELT treatment versus MPP^+ with those up-regulated during caloric restriction (p value = 0, FDR = 0, enrichment score = 1.30). Genes that are up-regulated by caloric restriction are also up-regulated by PSELT. Data were taken from GSE75569 [67].

E: Gene set enrichment analysis of a ranked list of all genes comparing MPP^+ and PSELT treatment versus MPP^+ with those up-regulated by resveratrol (p value = 0, enrichment score = 1.23). Genes that are up-regulated by resveratrol are also up-regulated by PSELT and inversely, genes down-regulated by resveratrol are also down-regulated by PSELT. Data were taken from GSE36930 [68] or from GSE36930 [68] and GSE42432 [69] in supplementary Fig. S1C.

F: Gene set enrichment analysis of a ranked list of all genes comparing MPP^+ and PSELT treatment versus MPP^+ with those associated/interacting with the transcription regulator EZH2 (p value = 0, enrichment score = −1.25). The EZH2-interacting genes are mostly correlated with PSELT treatment. Data were taken from the NCBI database (https://www.ncbi.nlm.nih.gov). **G:** Gene set enrichment analysis of a ranked list of all genes comparing MPP^+ and PSELT treatment versus MPP^+ with those up-regulated by EZH2 knockout (p value = 0, enrichment score = 1.14). Genes that are up-regulated by EZH2 knockout and have a H3K27me3 mark correlate with genes up-regulated by MPP^+ and are down-regulated by PSELT. Data were taken from GSE80222 [38] and from several other studies [70–72] in supplementary Fig. S1D. (For interpretation of the references to color in this figure legend, the reader is referred to the Web version of this article.)

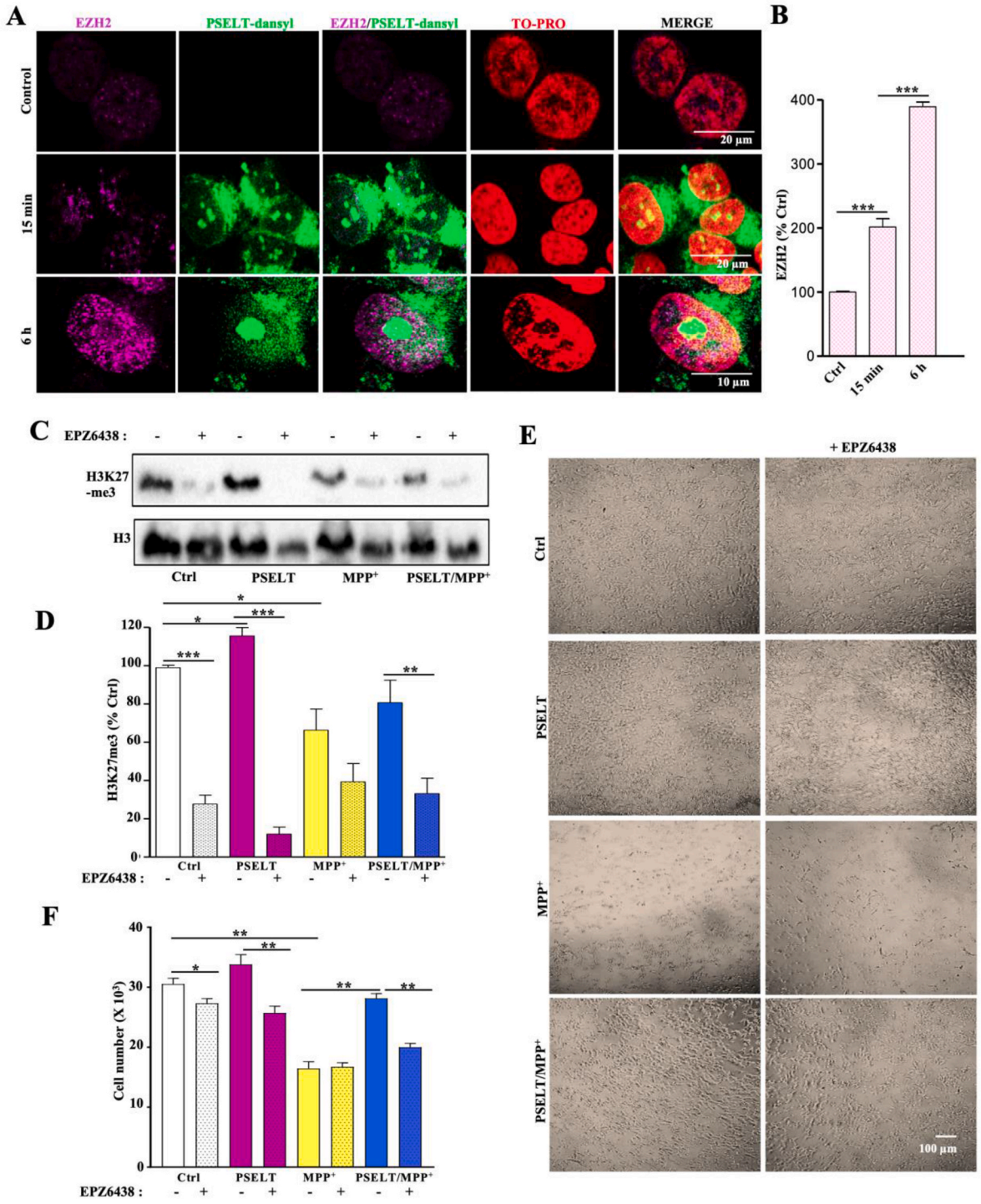

Fig. 8. PSELT regulates EZH2/H3K27me3 levels to promote cell survival.

A: SH-SY5Y cells were incubated with PSELT-dansyl for 15 min or 6 h and immunolabeled for EZH2. The nuclei were labeled by the TO-PRO dye. Scale bars: 10 and 20 µm

B: Quantification of EZH2 immunoreactivity after exposure to PSELT-dansyl. Data are expressed as mean ± SEM and are compared using Student *t*-test, $^{***}p < 0.001$ ($n = 3$ per condition).

C: Western blot analysis of H3K27me3 levels in SH-SY5Y cells treated or not with PSELT in the presence or absence of EPZ6438. The histone H3 levels were used as a protein loading control to normalize the data.

D: Quantification of H3K27me3 level after Western blot analysis of SH-SY5Y cells treated or not with PSELT in the presence or absence of EPZ6438. Data are expressed as mean ± SEM and are compared using ANOVA and Tukey's test, $^{*}p < 0.05$, $^{**}p < 0.01$, $^{***}p < 0.001$ ($n = 3$ per condition).

E: SH-SY5Y cells were treated by PSELT and MPP^+ in the presence or absence of EPZ6438. Scale bar: 100 µm.

F: Quantification of cell survival after PSELT and MPP^+ treatment in the presence or absence of EPZ6438. Data are expressed as mean ± SEM and are compared using ANOVA and Tukey's test, $^{*}p < 0.05$, $^{**}P < 0.01$ ($n = 3$ per condition). Experiments were repeated at least twice with similar results.

inhibitor significantly attenuates the pro-survival effect exerted by PSELT in the presence of MPP^+, indicating that the epigenetic regulator EZH2 is involved in the PSELT-promoted cell survival most likely by regulating histone methylation and chromatin remodeling.

3.7. PSELT ameliorates effects of MPTP on locomotor activity in mouse PD models

With these data showing an efficient dopaminergic neuron protection *in vitro* and *in vivo*, we explored possible motor benefits of PSELT after a progressive treatment with MPTP to model chronic neurodegeneration observed in PD. For this, we first analyzed mice coordination in the rotarod performance test at days 0, 2 and 7 when MPTP was injected daily at 30 mg/kg for 5 days and PSELT was simultaneously administered during 6 days as shown in Fig. 9A. Data analysis showed a clear beneficial effect of PSELT on motor coordination in the MPTP-treated animals at day 2 (Fig. 9B). At day 7, MPTP-treated animals recovered a coordination level comparable to that of controls and no effect of PSELT could be observed (Fig. S2A) in accordance with previous studies showing that PD animal models exhibit central compensatory phenomena after few days [40,41]. To further ascertain the beneficial effect of PSELT on motor skills, we assessed spontaneous locomotor activity of mice after MPTP treatment in the presence or absence of PSELT at days 0, 2 and 7 as described above (Fig. 9 C–H and Fig. S2). Thus, horizontal and vertical activities, and total distance traveled were recorded for the different animal groups using an automated device during 30 min in three 10-min periods, (Fig. 9 and Fig. S2, B-D). Data analysis of spontaneous activity during the 30-min period of recording revealed that control groups exhibit a slight, non-significant decrease of their activity due to habituation (Fig. 9, C, E and G) as previously reported [42]. Administration of MPTP (30 mg/kg) provoked a marked decrease in locomotor activity at day 2 of treatment (Fig. 9, D, F and H). Importantly, these MPTP-induced locomotor deficits observed at day 2 were significantly reduced after intranasal PSELT (30 μg/10 μl) treatment (Fig. 9, D, F and H), thus demonstrating that PSELT has motor benefits in this neurotoxin-induced Parkinson-like mouse model. At day 7, MPTP-treated mice recovered normal locomotor activity and no effect of PSELT could be observed (Fig. S2, B-D).

4. Discussion

Since its introduction in the 1960s, dopamine-replacement therapy (e.g., L-DOPA) has remained the leading treatment for PD. However, the effects of L-DOPA fade with disease progression and often results in side effects, including dyskinesias and motor fluctuations [43]. Various putative neuroprotective agents, including glial cell line-derived neurotrophic factor, brain-derived neurotrophic factor, transforming growth factor β and other small molecule compounds, have been assessed in different models of PD [44,45]. However, most of these compounds failed in either pre-clinical trials or human trials due to their inability to cross the blood-brain barrier or due to limited bioavailability. Moreover, they also caused adverse side effects. Therefore, effective minimally invasive treatment options that would slow or halt PD progression are still needed. Here, we believe the present study lends critical preclinical support for the use of PSELT as a new approach to protect dopaminergic neurons and to improve motor dysfunction in PD. Indeed, our results demonstrate that PSELT has several advantages in terms of efficacy and bioavailability since it targets oxidative stress at multiple intracellular sites and it easily crosses cell membranes after intranasal administration to protect dopaminergic neurons and their terminals, thus translating in motor skill improvement in a PD model.

Our previous findings showed that SELENOT, the selenoprotein from which PSELT was derived, exerts a potent protective effect on dopaminergic neurons and fibers of the nigrostriatal pathway, and that its conditional gene knockout in the mouse brain causes hyperactivity and higher vulnerability to neurotoxins such as rotenone and MPTP which profoundly affected this pathway and caused severe motor deficits [21,27]. We demonstrated in these previous studies that vector-based expression of SELENOT and not a selenocysteine-mutant form of the protein is able to promote cell survival, to restore TH levels and to prevent oxidative stress in neurotoxin-treated dopaminergic neurons, thus laying the way for the present study aimed at therapeutic application in PD. In addition, our earlier studies also showed that SELENOT is involved in the regulation of misfolded protein accumulation [29], mitochondrial function [46], calcium homeostasis and neurotransmitter release [21,26,28,47], different key cellular processes affected in PD [1] that could be improved by a SELENOT-based therapy.

To avoid the difficulties that may arise from the therapeutic use of a recombinant SELENOT protein which needs to cross the hematoencephalic barrier and could thus be rapidly degraded before it reaches the nigrostriatum in the brain, we reasoned that a short mimetic of the protein, namely PSELT, encompassing the active site with the CVSU motif may recapitulate the beneficial effects of SELENOT without the constraints that would be imposed by other parts of the protein that are required, for instance, for insertion in the ER membrane where it normally resides. We thus generated PSELT which was tested for its potential protective effect against MPP^+ toxicity. PSELT harboring the Sec and Cys residues was effective in promoting cell survival, inhibiting caspase 3 and preventing oxidative stress, indicating that PSELT is indeed able to mimic SELENOT and that the activity of this short peptide relies on the Sec/Cys-containing redox motif since the control peptide [Ser43,46]PSELT was devoid of effect. Although we have systematically seen a small increase in cell number following treatment by PSELT in basal condition, this effect was not significant. Therefore, PSELT does not seem to exert a significant effect on cell proliferation in contrast to the effect of SELENOT recently reported in SK-N-SH neuroblastoma cells [48]. This property of SELENOT observed in neuroblastoma cells is obviously not or poorly mimicked by PSELT.

Much to our surprise, confocal cell imaging and mass spectrometry analysis revealed that PSELT was able to cross the plasma membrane and to regulate the levels of various proteins located in the cytoplasm and within different subcellular compartments including the ER and the nuclei. This interesting finding indicated that PSELT is cell-permeable and could target oxidative stress in different cellular compartments, implying a multi-level redox impact. It should be noted that PSELT alone was as effective as PSELT conjugated with the cell-penetrating peptide TAT that we have also synthesized and tested for neuroprotective action, indicating that PSELT has a great intrinsic capacity to cross the plasma membrane. This property of PSELT represents an enormous advantage for its use as a therapeutic agent since the peptide could have access to various molecular targets in different compartments *in vivo* without the need for any additional vector. Indeed, our present results showed that PSELT is present in intracellular compartments of dopaminergic neurons in the SNc after intranasal administration, suggesting that the peptide acts at multiple subcellular levels *in vivo* as well. The structural basis of the cell-penetrating capacity of PSELT is not known yet and will be further investigated in future studies.

It is now recognized that oxidative stress is associated not only with the aging brain but may also play an important pathophysiological role in the development of PD [7,49,50]. For instance, the relevance of oxidative stress to the pathogenesis of PD is supported by the fact that genes whose mutation causes the disease such as α-synuclein, DJ-1, LRKK2 and parkin [51] are all linked to oxidative stress [52,53]. However, attempts to exploit the systemic oxidative stress therapeutically and to improve disease outcome by using antioxidants have been ineffective or even harmful [12]. The reasons for these failures are starting to be understood and involve the undefined nature of pathological oxidative stress and the dysregulation of complex networks of proteins and other macromolecules leading to irreversible degradation of neurons and synapses in the brain of affected subjects. In this context, current approaches to tackle harmful oxidative stress is to target disease-relevant enzymatic sources of ROS or alternatively to

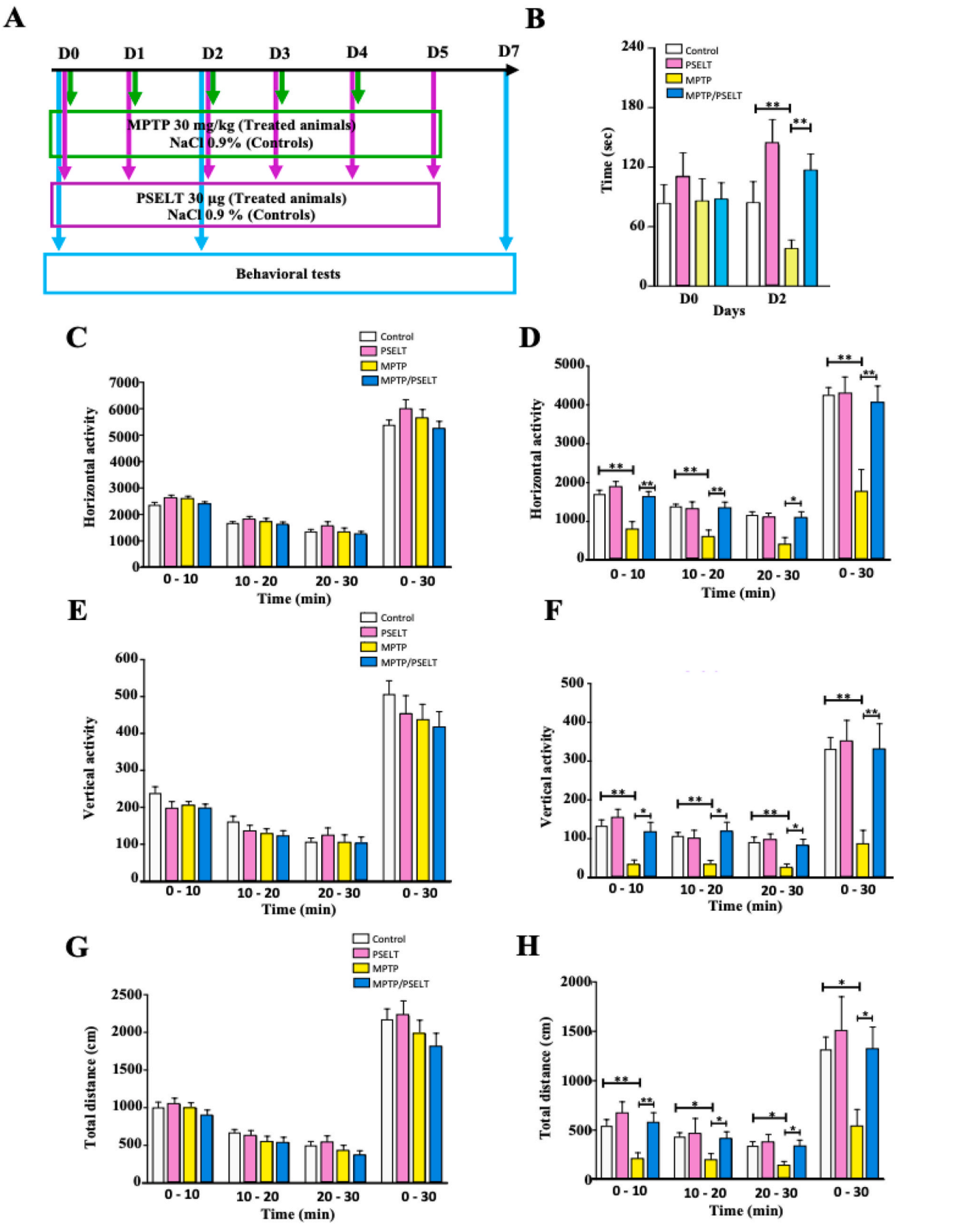

(caption on next page)

Fig. 9. PSELT ameliorates motor activity after MPTP treatment.
A: Schematic representation of the protocol used for MPTP and PSELT treatments. Animals received 1 dose of MPTP (30 mg/kg) or NaCl 0.9% (controls) intraperitoneally each day for 5 days. PSELT was administered (30 μg/animal) intranasally each day for 6 days. Behavioral tests were performed at days 0, 2 and 7. Results of behavioral tests recorded at day 7 are shown as supplemental data (Fig. S2) and only data from days 0 and 2 are shown here.
B: The coordination capacity of the animal groups was monitored using a rotarod. The latency at which the mice were able to maintain their balance on the bar was recorded. The average latency of the last two trials was used for analyses. Data are expressed as mean ± SEM and are compared using Student *t*-test, $^{**}p < 0.01$ ($n = 12$).
C and D: Horizontal activity of all animal groups was recorded during 3 consecutive periods of 10 min at days 0 (C) and 2 (D). Total horizontal activity for 30 min is shown for each animal group. Data are expressed as mean ± SEM and are compared using Student *t*-test, $^{*}p < 0.05$, $^{**}p < 0.01$ ($n = 12$).
E and F: Vertical activity of all animal groups was monitored during 3 consecutive periods of 10 min at days 0 (E) and 2 (F). Data are expressed as mean ± SEM and are compared using Student *t*-test, $^{*}p < 0.05$, $^{**}p < 0.01$ ($n = 12$)
G and H: Total distance traveled by all animals was recorded in 3 consecutive periods of 10 min at days 0 (G) and 2 (H). Data are expressed as mean ± SEM and are compared using Student *t*-test, $^{*}p < 0.05$, $^{**}p < 0.01$ ($n = 12$).

functionally repair oxidatively damaged proteins [12]. In this regard, PSELT which derives from the ROS-inhibiting and proteostasis-supporting enzyme SELENOT and which could regenerate active macromolecules in oxidative stress conditions through its reducing activity mediated by the selenyl-thiol bridge may represent an attractive therapeutic candidate. This implies that PSELT would exert its protective effects by reducing different cellular components that would recover their function, a hypothesis that will need to be substantiated in future studies. Nevertheless, our previous findings showing that SELENOT contributes to the posttranslational maturation of ER-transiting proteins through its redox activity and probably covalent bridge alteration in the client proteins [29] support the idea that PSELT could exert such effect in multiple subcellular compartments. In accordance, our microarray analyses showed that PSELT treatment leads to the modulation of the expression of a number of genes associated with PD, probably by affecting the regulatory function of several factors via redox mechanisms. Among these, PSELT could trigger a transcriptional adaptive response through epigenetic regulation led by EZH2/H3K27me3 to promote cell survival. Indeed, inhibition of this regulatory pathway interfered with PSELT-induced cell survival. This latter finding is in line with recent reports demonstrating the importance of epigenetic regulation in neurodegeneration and neuroprotection [54] and highlights a previously unknown relationship between antioxidant activity and epigenetic regulation of cell survival. It should be noted that MPP^+ has its own inhibitory effect on H3K27me3 and that addition of EZH2 inhibitor had no additional effect in the presence of MPP^+, which indicates that the effect of the latter on H3K27me3 level is independent of EZH2 and is probably not involved in cell survival. Indeed, administration of EZH2 inhibitor did not modify MPP^+-induced cell death, while the inhibitor which down-regulates H3K27me3 reversed the effect of PSELT on both H3K27me3 and cell survival, thus supporting our conclusion that PSELT regulates EZH2/H3K27me levels to promote cell survival although PSELT did not revert the effect of MPP^+ on H3K27me3 which is probably not related to cell survival. Proteomic studies will be required to determine how PSELT modifies directly or via other factors EZH2 in order to trigger neuroprotection under oxidative stress condition. It is important to note that PSELT adaptive response in MPP^+-treated neuroblastoma cells correlated with expression of gene sets associated with different neurodegenerative diseases or neurogenesis (present data and other unpublished observations), indicating that PSELT and probably epigenetic regulation also could represent useful therapeutic options in various brain pathologies.

Most importantly, PSELT treatment protected against nigral dopaminergic neuronal damage and motor deficits in animal models of PD. Routing of PSELT to the nigrostriatal pathway in the MPTP animal model could be achieved upon intranasal administration, thus bypassing the blood-brain barrier and therefore offering a non-invasive way of treatment for this novel therapy in PD. This therapeutic route [55] and similar doses compared to the one chosen for PSELT in the present study (30 μg/10 μl/animal) were successfully used in preclinical models for the treatment of different brain diseases with appropriate agents including insulin-like growth factor for Huntington disease [56], granulocyte colony-stimulating factor for ischemia [57] or EGF for neonatal brain injury [58]. No toxicity or behavioral imparities compared to control mice were observed upon treatment with the dose used of PSELT, although additional studies will be required to further document PSELT pharmacological properties. The peptide was effective in improving motor function in mice treated with MPTP in the early phase of neurodegeneration, supporting the potential therapeutic efficacy of this peptide. However, in the protocols used to induce neurodegeneration in mice, there are inevitably compensatory mechanisms that take place in the brain after few days of neurotoxin treatment [40, 59] which mask the long-term effect of PSELT and the potential to alleviate durably motor impairments. In fact, PSELT exhibited a clear trend to normalize dopamine levels in the striatum after 7 days of treatment but the differences were not statistically significant likely due to the compensation phenomena. Nevertheless, PSELT was able to normalize TH and phosphorylated TH levels, which should impact dopamine synthesis at the long term but other processes such as storage and exocytosis of the neurotransmitter may also be affected in this disease model.

Despite the limitations of the animal model, it is interesting to note that PSELT regulates the levels of proteins that are mutated in PD such as α-synuclein and DJ-1, suggesting that PSELT could impact pathways that are affected in human disease. Given the complexity of the effects of oxidative stress-induced neurodegeneration, the elucidation of these pathways is challenging at this point although pinpointing EZH2 as a major target is an important finding towards this goal.

In conclusion, our study provides direct evidence that targeting dopaminergic neurons and terminals using the small mimetic PSELT is feasible and potentially applicable to the treatment of PD. Because PSELT is a cell-penetrating, polyfunctional peptide that targets cell-wide oxidative stress, it is a promising therapeutic candidate for PD and probably other neurodegenerative diseases. It is tempting to speculate that PSELT, and not other antioxidants, is also acting to prevent misfolding of oxidized biomolecules, thus attenuating oxidative and ER stress. In fact, PSELT is probably acting as an efficient thioredoxin-like entity that helps proteins to cope with oxidative stress. It is noteworthy that PSELT displayed comparable effects on gene expression to those of resveratrol as revealed by the microarray analysis. Resveratrol is a widely used antioxidant and anti-inflammatory phytoalexin which holds several health-promoting activities [60]. However, since resveratrol exhibits rapid metabolism and limited systemic bioavailability [60], PSELT may represent an interesting therapeutic alternative that can be applied to combat the major culprit in neurodegeneration represented by oxidative stress.

Author contributions

I.A. and L.B. carried out most experiments. B.L. and J.L. performed peptide synthesis and mass spectrometry analyses. D.G. helped with imaging experiments. J.A-L. and C.B. performed epigenetic studies. J-L. dR., J-C.dR. and D.M. helped with behavioral studies and their interpretation. A.A., F.N., A.B. and A.C. helped with *in vivo* experiments. A.E.

and L.E.E performed, analyzed and interpreted the microarray data. Y.A. conceived the project, analyzed data, and wrote the manuscript with input from all coauthors.

Declaration of competing interest

There is no conflict of interest.

Acknowledgements

This work was supported by the Institut National de la Santé et de la Recherche Médicale (INSERM, grant number U1239 to YA); University of Rouen Normandie (Grant DC2N to YA); the Regional Council of Normandy and the European Community FEDER program (Europe gets involved in regional development through the ERDF program) (Grants DO-IT, PACT-PACT-PACBS and PHEDERCPG to YA); the Comparative Genomics and Cancer Genetics Branch, National Human Genome Research Institute, National Institutes of Health (to AGE) and the Ministry of Education of Saudi Arabia (Scholarship to I.A.). Images were acquired and peptides were synthesized in PRIMACEN, the cell imaging platform of Normandy and behavioral analyses were performed in the SCAC platform of IRIB. The funders had no role in study design, data collection and analysis, decision to publish, or preparation of the manuscript.

Appendix A. Supplementary data

Supplementary data to this article can be found online at https://doi.org/10.1016/j.redox.2020.101839.

References

[1] J.A. Obeso, M. Stamelou, C.G. Goetz, W. Poewe, A.E. Lang, D. Weintraub, D. Burn, G.M. Halliday, E. Bezard, S. Przedborski, S. Lehericy, D.J. Brooks, J.C. Rothwell, M. Hallett, M.R. DeLong, C. Marras, C.M. Tanner, G.W. Ross, J.W. Langston, C. Klein, V. Bonifati, J. Jankovic, A.M. Lozano, G. Deuschl, H. Bergman, E. Tolosa, M. Rodriguez-Violante, S. Fahn, R.B. Postuma, D. Berg, K. Marek, D.G. Standaert, D.J. Surmeier, C.W. Olanow, J.H. Kordower, P. Calabresi, A.H.V. Schapira, A. J. Stoess, Past, present, and future of Parkinson's disease: a special essay on the 200th Anniversary of the Shaking Palsy, Mov. Disord. 32 (2017) 1264–1310.
[2] A.D. Macleod, K.S. Taylor, C.E. Counsell, Mortality in Parkinson's disease: a systematic review and meta-analysis, Mov. Disord. 29 (2014) 1615–1622.
[3] M. Bisaglia, E. Greggio, M. Beltramini, L. Bubacco, Dysfunction of dopamine homeostasis: clues in the hunt for novel Parkinson's disease therapies, Faseb. J. 27 (2013) 2101–2110.
[4] S.R. Subramaniam, M.F. Chesselet, Mitochondrial dysfunction and oxidative stress in Parkinson's disease, Prog. Neurobiol. 106–107 (2013) 17–32.
[5] M.S. Hipp, P. Kasturi, F.U. Hartl, The proteostasis network and its decline in ageing, Nat. Rev. Mol. Cell Biol. 20 (2019) 421–435.
[6] D.J. Surmeier, J.N. Guzman, J. Sanchez-Padilla, J.A. Goldberg, The origins of oxidant stress in Parkinson's disease and therapeutic strategies, Antioxidants Redox Signal. 14 (2011) 1289–1301.
[7] B.G. Trist, D.J. Hare, K.L. Double, Oxidative stress in the aging substantia nigra and the etiology of Parkinson's disease, Aging Cell 18 (2019), e13031.
[8] O. Hwang, Role of oxidative stress in Parkinson's disease, Exp. Neurobiol. 22 (2013) 11–17.
[9] P. Jenner, C.W. Olanow, Oxidative stress and the pathogenesis of Parkinson's disease, Neurology 47 (1996) S161–S170.
[10] V.T. Dao, A.I. Casas, G.J. Maghzal, T. Seredenina, N. Kaludercic, N. Robledinos-Anton, F. Di Lisa, R. Stocker, P. Ghezzi, V. Jaquet, A. Cuadrado, H.H. Schmidt, Pharmacology and clinical drug candidates in redox medicine, Antioxidants Redox Signal. 23 (2015) 1113–1129.
[11] P. Ghezzi, V. Jaquet, F. Marcucci, H.H.H.W. Schmidt, The oxidative stress theory of disease: levels of evidence and epistemological aspects, Br. J. Pharmacol. 174 (2017) 1784–1796.
[12] A.I. Casas, D.V. Dao, A. Daiber, G.J. Maghzal, F. Di Lisa, N. Kaludercic, S. Leach, A. Cuadrado, V. Jaquet, T. Seredenina, K.H. Krause, M.G. López, R. Stocker, P. Ghezzi, H.H. Schmidt, Reactive oxygen-related diseases: therapeutic targets and emerging clinical indications, Antioxidants Redox Signal. 23 (2015) 1171–1185.
[13] M. Szelechowski, A. Bétourné, Y. Monnet, C.A. Ferré, A. Thouard, C. Foret, J. M. Peyrin, S. Hunot, D. Gonzalez-Dunia, A viral peptide that targets mitochondria protects against neuronal degeneration in models of Parkinson's disease, Nat. Commun. 5 (2014) 5181.
[14] M.S. Gorbatyuk, A. Shabashvili, W. Chen, C. Meyers, L.F. Sullivan, M. Salganik, J. H. Lin, A.S. Lewin, N. Muzyczka, O.S. Gorbatyuk, Glucose regulated protein 78 diminishes α-synuclein neurotoxicity in a rat model of Parkinson disease, Mol. Ther. 20 (2012) 1327–1337.
[15] S. Altenhofer, P.W. Kleikers, K.A. Radermacher, P. Scheurer, J.J. Rob Hermans, P. Schiffers, H. Ho, K. Wingler, H.H. Schmidt, The NOX toolbox: validating the role of NADPH oxidases in physiology and disease, Cell. Mol. Life Sci. 69 (2012) 2327–2343.
[16] I. Ferrer, A. Martinez, R. Blanco, E. Dalfó, M. Carmona, Neuropathology of sporadic Parkinson disease before the appearance of parkinsonism: preclinical Parkinson disease, J. Neural. Transm. 118 (2011) 821–839.
[17] H. Xie, S. Hou, J. Jiang, M. Sekutowicz, J. Kelly, B.J. Bacskai, Rapid cell death is preceded by amyloid plaque-mediated oxidative stress, Proc. Natl. Acad. Sci. *U*.S.A. 1*10* (2013) 7904–7909.
[18] V.M. Labunskyy, D.L. Hatfield, V.N. Gladyshev, Selenoproteins: molecular pathways and physiological roles, Physiol. Rev. 94 (2014) 739–777.
[19] J.A. Obeso, M.C. Rodriguez-Oroz, C.G. Goetz, C. Marin, J.H. Kordower, M. Rodriguez, E.C. Hirsch, M. Farrer, A.H. Schapira, G. Halliday, Missing pieces in the Parkinson's disease puzzle, Nat. Med. 16 (2010) 653–661.
[20] J.A. Goldberg, J.N. Guzman, C.M. Estep, E. Ilijic, J. Kondapalli, J. Sanchez-Padilla, D.J. Surmeier, Calcium entry induces mitochondrial oxidant stress in vagal neurons at risk in Parkinson's disease, Nat. Neurosci. 15 (2012) 1414–1421.
[21] L. Boukhzar, A. Hamieh, D. Cartier, Y. Tanguy, I. Alsharif, M. Castex, A. Arabo, S. El Hajji, J.J. Bonnet, M. Errami, A. Falluel-Morel, A. Chagraoui, I. Lihrmann, Y. Anouar, Selenoprotein T exerts an essential oxidoreductase activity that protects dopaminergic neurons in mouse models of Parkinson's disease, Antioxidants Redox Signal. 24 (2016) 557–574.
[22] S. Seeher, B.A. Carlson, A.C. Miniard, E.K. Wirth, Y. Mahdi, D.L. Hatfield, D. M. Driscoll, U. Schweizer, Impaired selenoprotein expression in brain triggers striatal neuronal loss leading to coordination defects in mice, Biochem. J. 462 (2014) 67–75.
[23] E.K. Wirth, M. Conrad, J. Winterer, C. Wozny, B.A. Carlson, S. Roth, D. Schmitz, G. W. Bornkamm, V. Coppola, L. Tessarollo, L. Schomburg, J. Köhrle, D.L. Hatfield, U. Schweizer, Neuronal selenoprotein expression is required for interneuron development and prevents seizures and neurodegeneration, Faseb. J. 24 (2010) 844–852.
[24] L. Arodin, A. Miranda-Vizuete, P. Swoboda, A.P. Fernandes, Protective effects of the thioredoxin and glutaredoxin systems in dopamine-induced cell death, Free Radic. Biol. Med. 73 (2014) 328–336.
[25] F.P. Bellinger, M.T. Bellinger, L.A. Seale, A.S. Takemoto, A.V. Raman, T. Miki, A. B. Manning-Boğ, M.J. Berry, L.R. White, G.W. Ross, Glutathione peroxidase 4 is associated with neuromelanin in substantia nigra and dystrophic axons in putamen of Parkinson's brain, Mol. Neurodegener. 6 (2011) 8.
[26] Y. Anouar, I. Lihrmann, A. Falluel-Morel, L. Boukhzar, Selenoprotein T is a key player in ER proteostasis, endocrine homeostasis and neuroprotection, Free Radic. Biol. Med. 127 (2018) 145–152.
[27] M.T. Castex, A. Arabo, M. Bénard, V. Roy, V. Le Joncour, G. Prévost, J.J. Bonnet, Y. Anouar, A. Falluel-Morel, Selenoprotein T deficiency leads to neurodevelopmental abnormalities and hyperactive behavior in mice, Mol. Neurobiol. 53 (2016) 5818–5832.
[28] L. Grumolato, H. Ghzili, M.M. Montero-Hadjadje, S. Gasman, J. Lesage, Y. Tanguy, L. Galas, D. Ait-Ali, J. Leprince, N.C. Guérineau, A.G. Elkahloun, A. Fournier, D. Vieau, H. Vaudry, Y. Anouar, Selenoprotein T is a PACAP-regulated gene involved in intracellular Ca^{2+} mobilization and neuroendocrine secretion, Faseb. J. 22 (2008) 1756–1768.
[29] A. Hamieh, D. Cartier, H. Abid, A. Calas, C. Burel, C. Bucharles, C. Jehan, L. Grumolato, M. Landry, P. Lerouge, Y. Anouar, I. Lihrmann, Selenoprotein T is a novel OST subunit that regulates UPR signaling and hormone secretion, EMBO Rep. 18 (2017) 1935–1946.
[30] Varlamova, E.G. Protein-protein interactions of ER-resident selenoproteins with their physiological partners. Biochimie 171–172, 197-204.
[31] A. Touchard, S.R. Aili, N. Téné, V. Barassé, C. Klopp, A. Dejean, Kini, R. M. Mrinalini, L. Coquet, T. Jouenne, B. Lefranc, J. Leprince, P. Escoubas, G. M. Nicholson, M. Treilhou, E. Bonnafé, Venom peptide repertoire of the European Myrmicine ant Manica rubida: identification of insecticidal toxins, J. Proteome Res. 19 (2020) 1800–1811.
[32] Broad molecular signatures database v5.0 (MSigDB). http://www.broadinstitute.org/gsea/.
[33] V.K. Mootha, C.M. Lindgren, K.-F. Eriksson, A. Subramanian, S. Sihag, J. Lehar, P. Puigserver, E. Carlsso, M. Ridderstråle, E. Laurila, N. Houstis, M.J. Daly, N. Patterson, J.P. Mesirov, T.R. Golub, P. Tamayo, B. Spiegelman, E.S. Lander, J. N. Hirschhorn, D. Altshuler, L.C. Groop, PGC-1α-responsive genes involved in oxidative phosphorylation are coordinately downregulated in human diabetes, Nat. Genet. 34 (2003) 267–273.
[34] A. Subramanian, P. Tamayo, V.K. Mootha, S. Mukherjee, B.L. Ebert, M.A. Gillette, A. Paulovich, S.L. Pomeroy, T.R. Golub, E.S. Lander, J.P. Mesirov, Gene set enrichment analysis: a knowledge-based approach for interpreting genome-wide expression profiles, Proc. Natl. Acad. Sci. U. S. A. 102 (2005) 15545–15550.
[35] H. Ariga, K. Takahashi-Niki, I. Kato, H. Maita, T. Niki, S.M. Iguchi-Ariga, Neuroprotective Function of DJ-1 in Parkinson's Disease, 2013, 683920.
[36] A. Dumitriu, J. Golji, A.T. Labadorf, B. Gao, T.G. Beach, R.H. Myers, K.A. Longo, J. C. Latourelle, Integrative analyses of proteomics and RNA transcriptomics implicate mitochondrial processes, protein folding pathways and GWAS loci in Parkinson disease, BMC Med. Genom. 9 (2016) 5.
[37] V.L. Truong, M. Jun, W.S. Jeong, Role of resveratrol in regulation of cellular defense systems against oxidative stress, Biofactors 44 (2018) 36–49.

[38] X. Feng, A.H. Juan, H.A. Wang, K.D. Ko, H. Zare, V. Sartorelli, Polycomb Ezh2 controls the fate of GABAergic neurons in the embryonic cerebellum, Development 143 (2016) 1971–1980.
[39] A. Batool, C. Jin, Y.-X. Liu, Role of EZH2 in cell lineage determination and relative signaling pathways, Front. Biosci. 24 (2019) 947–960.
[40] E. Bezard, S. Dovero, C. Imbert, T. Boraud, C.E. Gross, Spontaneous long-term compensatory dopaminergic sprouting in MPTP-treated mice, Synapse 38 (2000) 363–368.
[41] D. Domenger, D. Dea, L. Theroux, L. Moquin, A. Gratton, J. Poirier, The MPTP neurotoxic lesion model of Parkinson's disease activates the apolipoprotein E cascade in the mouse brain, Exp. Neurol. 233 (2012) 513–522.
[42] M.P. Leussis, V.J. Bolivar, Habituation in rodents: a review of behavior, neurobiology, and genetics, Neurosci. Biobehav. Rev. 30 (2006) 1045–1064.
[43] U.J. Kang, S. Fahn, Management of tardive dyskinesia, Ration. Drug Ther. 22 (1988) 1–7.
[44] X. Su, A.P. Kells, E.J. Huang, H.S. Lee, P. Hadaczek, J. Beyer, J. Bringas, P. Pivirotto, J. Penticuff, J. Eberling, H.J. Federoff, J. Forsayeth, K.S. Bankiewicz, Safety evaluation of AAV2-GDNF gene transfer into the dopaminergic nigrostriatal pathway in aged and parkinsonian rhesus monkeys, Hum. Gene Ther. 20 (2009) 1627–1640.
[45] J.H. Kordower, M.E. Emborg, J. Bloch, S.Y. Ma, Y. Chu, L. Leventhal, J. McBride, E. Y. Chen, S. Palfi, B.Z. Roitberg, W.D. Brown, J.E. Holden, R. Pyzalski, M.D. Taylor, P. Carvey, Z. Ling, D. Trono, P. Hantraye, N. Déglon, P. Aebischer, Neurodegeneration prevented by lentiviral vector delivery of GDNF in primate models of Parkinson's disease, Science 290 (2000) 767–773.
[46] H. Abid, D. Cartier, A. Hamieh, A.M. François-Bellan, C. Bucharles, H. Pothion, D. L. Manecka, J. Leprince, A. Adriouch, O. Boyer, Y. Anouar, I. Lihrmann, AMPK activation of PGC-1α/NRF-1-dependent SELENOT gene transcription promotes PACAP-induced neuroendocrine cell differentiation through tolerance to oxidative stress, Mol. Neurobiol. 56 (2019) 4086–4101.
[47] G. Prevost, A. Arabo, L. Jian, E. Quelennec, D. Cartier, S. Hassan, A. Falluel-Morel, Y. Tanguy, S. Gargani, I. Lihrmann, J. Kerr-Conte, H. Lefebvre, F. Pattou, Y. Anouar, The PACAP-regulated gene selenoprotein T is abundantly expressed in mouse and human β-cells and its targeted inactivation impairs glucose tolerance, Endocrinology 154 (2013) 3796–3806.
[48] Z. Shao, X. Zhang, H.H. Fan, X. Wang, H. Wu, L. Zhang, W. Cheng, J. Zhu, Selenoprotein T promotes proliferation and G1-to-S transition in SK-N-SH cells: implications in Parkinson's disease, J. Nutr. 149 (2019) 2110–2119.
[49] T. Jiang, Q. Sun, S. Chen, Oxidative stress: a major pathogenesis and potential therapeutic target of antioxidative agents in Parkinson's disease and Alzheimer's disease, Prog. Neurobiol. 147 (2016) 1–19.
[50] Yeung, A.W.K., Tzvetkov, N.T., Georgieva, M.G., Ognyanov, I.V., Kordos, K., Jóźwik, A., Kühl, T., Perry, G., Petralia, M.C., Mazzon, E., and Atanasov, A. Reactive oxygen species (ROS) and their impact in neurodegenerative diseases: literature landscape analysis. Antioxidants Redox Signal. (ePub ahead of print 2020). PMID: 32030995 DOI: 10.1089/ars.2019.7952.
[51] M.A. Nalls, V. Plagnol, D.G. Hernandez, M. Sharma, U.M. Sheerin, M. Saad, J. Simón-Sánchez, C. Schulte, S. Lesage, S. Sveinbjörnsdóttir, K. Stefánsson, M. Martinez, J. Hardy, P. Heutink, A. Brice, T. Gasser, A.B. Singleton, N.W. Wood, Imputation of sequence variants for identification of genetic risks for Parkinson's disease: a meta-analysis of genome-wide association studies, Lancet 377 (2011) 641–649.
[52] T.M. Dawson, V.L. Dawson, The role of parkin in familial and sporadic Parkinson's disease, Mov. Disord. 25 (2010) S32–S39.
[53] V. Dias, E. Junn, M.M. Mouradian, The role of oxidative stress in Parkinson's disease, J. Parkinsons Dis. 3 (2013) 461–491.
[54] J.Y. Hwang, K.A. Aromolaran, R.S. Zukin, The emerging field of epigenetics in neurodegeneration and neuroprotection, Nat. Rev. Neurosci. 18 (2017) 347–361.
[55] A.E.-E. Aly, B.L. Waszczak, Intranasal gene delivery for treating Parkinson's disease: overcoming the blood-brain barrier, Expet Opin. Drug Deliv. 12 (2015) 1923–1941.
[56] C. Lopes, M. Ribeiro, A.I. Duarte, S. Humbert, F. Saudou, L. Pereira de Almeida, M. Hayden, A.C. Rego, IGF-1 intranasal administration rescues Huntington's disease phenotypes in YAC128 Mice, Mol. Neurobiol. 49 (2014) 1126–1142.
[57] B.-L. Sun, M.-Q. He, X.-Y. Han, J.-Y. Sun, M.-F. Yang, H. Yuan, C.-D. Fan, S. Zhang, L.-L. Mao, D.-W. Li, Z.-Y. Zhang, C.-B. Zheng, X.-Y. Yang, Y.V. Li, R.A. Stetler, J. Chen, F. Zhang, Intranasal delivery of granulocyte colony-stimulating factor enhances its neuroprotective effects against ischemic brain injury in rats, Mol. Neurobiol. 53 (2016) 320–330.
[58] J. Scafidi, T.R. Hammond, S. Scafidi, J. Ritter, B. Jablonska, M. Roncal, K. Szigeti-Buck, D. Coman, Y. Huang, R.J. McCarter Jr., F. Hyder, T.L. Horvath, V. Gallo, Intranasal epidermal growth factor treatment rescues neonatal brain injury, Nature 506 (2014) 230–234.
[59] J. Blesa, I. Trigo-Damas, M. Dileone, N.L. Del Rey, L.F. Hernandez, J.A. Obeso, Compensatory mechanisms in Parkinson's disease: circuits adaptations and role in disease modification, Exp. Neurol. 298 (2017) 148–161.
[60] A.P. Singh, R. Singh, S.S. Verma, V. Rai, C.H. Kaschula, P. Maiti, S.C. Gupta, Health benefits of resveratrol: evidence from clinical studies, Med. Res. Rev. 39 (2019) 1851–1891.
[61] A. Vardi, H. Zigdon, A. Meshcheriakova, A.D. Klein, C. Yaacobi, B.M. Kenwood, A. A. Rahim, G. Massaro, A.H. Merrill, E.B. Vitner, A.H. Futerman, Delineating pathological pathways in a chemically induced mouse model of Gaucher disease, J. Pathol. 239 (2016) 496–509.
[62] D.C. Duke, L.B. Moran, R.K. Pearce, M.B. Graeber, The medial and lateral substantia nigra in Parkinson's disease: mRNA profiles associated with higher brain tissue vulnerability, Neurogenetics 8 (2007) 83–94.
[63] S. Laguesse, C. Creppe, D.D. Nedialkova, P.P. Prévot, Borgs, S. Huysseune, B. Franco, G. Duysens, N. Krusy, G. Lee, N. Thelen, M. Thiry, P. Close, A. Chariot, B. Malgrange, S.A. Leidel, J.D. Godin, L. Nguyen, A dynamic unfolded protein response contributes to the control of cortical neurogenesis, Dev. Cell 35 (2015) 553–567.
[64] B. Juliandi, K. Tanemura, K. Igarashi, T. Tominaga, Y. Furukawa, M. Otsuka, D. Ikegami, M. Abematsu, T. Sanosaka, K. Tsujimura, M. Narita, J. Kanno, K. Nakashima, Reduced adult hippocampal neurogenesis and cognitive impairments following prenatal treatment of the antiepileptic drug valproic acid, Stem. Cell. Rep. 5 (2015) 996–1009.
[65] A. Fernández-Medarde, A. Porteros, J. de las Rivas, A. Núñez, J.J. Fuster, E. Santos, Laser microdissection and microarray analysis of the hippocampus of Ras-GRF1 knockout mice reveals gene expression changes affecting signal transduction pathways related to memory and learning, Neuroscience 146 (2007) 272–285.
[66] D.A. Kozareva, O.F. O'Leary, J.F. Cryan, Y.M. Nolan, Deletion of TLX and social isolation impairs exercise-induced neurogenesis in the adolescent hippocampus, Hippocampus 28 (2018) 3–11.
[67] J.L. Barger, J.M. Vann, N.L. Cray, T.D. Pugh, A. Mastaloudis, S.N. Hester, S. M. Wood, M.A. Newton, R. Weindruch, T.A. Prolla, Identification of tissue-specific transcriptional markers of caloric restriction in the mouse and their use to evaluate caloric restriction mimetics, Aging Cell 16 (2017) 750–760.
[68] J. Tomé-Carneiro, M. Gonzálvez, M. Larrosa, F.J. Yáñez-Gascón, J.A. Ruiz-Ros, F. A. Tomás-Barberán, M.T. García-Conesa, J.C. Espín, Grape resveratrol increases serum adiponectin and downregulates inflammatory genes in peripheral blood mononuclear cells: a triple-blind, placebo-controlled, one-year clinical trial in patients with stable coronary artery disease, Cardiovasc. Drugs Ther. 27 (2013) 37–48.
[69] E. Konings, S. Timmers, M.V. Boekschoten, G.H. Goossens, J.W. Jocken, L. A. Afman, M. Müller, P. Schrauwen, L.A. Mariman, E.E. Blaak, The effects of 30 days resveratrol supplementation on adipose tissue morphology and gene expression patterns in obese men, Int. J. Obes. 38 (2014) 470–473.
[70] M. Nuytten, L. Beke, A. Van Eynde, H. Ceulemans, M. Beullens, P. Van Hummelen, F. Fuks, M. Bollen, The transcriptional repressor NIPP1 is an essential player in EZH2-mediated gene silencing, Oncogene 27 (2008) 1449–1460.
[71] E. Missiaglia, M. Donadelli, M. Palmieri, T. Crnogorac-Jurcevic, A. Scarpa, N. R. Lemoine, Growth delay of human pancreatic cancer cells by methylase inhibitor 5-aza-2'-deoxycytidine treatment is associated with activation of the interferon signaling pathway, Oncogene 24 (2005) 199–211.
[72] C. Lu, H.D. Han, L.S. Mangala, R. Ali-Fehmi, C.S. Newton, L. Ozbun, G.N. Armaiz-Pena, W. Hu, R.L. Stone, A. Munkarah, M.K. Ravoori, M.M. Shahzad, J.W. Lee, E. Mora, R.R. Langley, A.R. Carroll, K. Matsuo, W.A. Spannuth, R. Schmandt, N. B. Ennings, B.W. Goodman, R.B. Jaffe, A.M. Nick, H.S. Kim, E.O. Guven, Y.H. Chen, L.Y. Li, M.C. Hsu, R.L. Coleman, G.A. Calin, E.B. Denkbas, J.Y. Lim, J.S. Lee, V. Kundra, M.J. Birrer, M.C. Hung, G. Lopez-Berestein, A.K. Sood, Regulation of tumor angiogenesis by EZH2, Canc. Cell 18 (2010) 185–197.